Advances in organ-on-a-chip engineering

Boyang Zhang[1], *Anastasia Korolj*[1,2], *Benjamin Fook Lun Lai*[1] *and Milica Radisic*[1,2,3,4]*

Abstract | Predicting the effects of drugs before human clinical trials is at the heart of drug screening and discovery processes. The cost of drug discovery is steadily increasing owing to the limited predictability of 2D cell culture and animal models. The convergence of microfabrication and tissue engineering gave rise to organ-on-a-chip technologies, which offer an alternative to conventional preclinical models for drug screening. Organ-on-a-chip devices can replicate key aspects of human physiology crucial for the understanding of drug effects, improving preclinical safety and efficacy testing. In this Review, we discuss how organ-on-a-chip technologies can recreate functions of organs, focusing on tissue barrier properties, parenchymal tissue function and multi-organ interactions, which are three key aspects of human physiology. Specific organ-on-a-chip systems are examined in terms of cell sources, functional hallmarks and available disease models. Finally, we highlight the challenges that need to be overcome for the clinical translation of organ-on-a-chip devices regarding materials, cellular fidelity, multiplexing, sensing, scalability and validation.

Adverse drug events causing emergency department visits were estimated to occur as frequently as 4 in every 1,000 patients in 2013–2014 in the United States[1]. Cardiac and liver toxicity are the leading causes of post-approval drug withdrawals, and many other drugs fail owing to a lack of efficacy and a poor understanding of the mechanism of action. Moreover, up to 20% of acute kidney injuries acquired after hospital admissions are attributed to drug-induced nephrotoxicity not predicted by preclinical models[2,3]. In addition to the many failures of marketed drugs, the number of new drugs approved annually has also decreased over the past 20 years, raising concerns over a 'drying pipeline'[4–7]. It is becoming increasingly clear that the cell lines and animal models currently used for drug development and testing fall short in predicting the pathophysiology of human disease, personalized drug sensitivities of specific patient subgroups and off-target drug toxicity. For example, patient-derived tumour xenografts can undergo murine-specific tumour evolution when implanted in mice, questioning the validity of animal testing for cancer therapy[8]. Furthermore, the development of drugs for conditions affecting prenatal and newly born humans remains unaddressed owing to a lack of suitable models. It is also important to investigate teratogenic effects of drugs and environmental chemicals in the increasingly polluted world, which is currently not possible in humans. Therefore, new methods and approaches for drug discovery and health research are required.

One of the first papers detailing the use of organized cell cultures to study disease was published by Andre Kleber in 1991, reporting the construction of a ventricular myocardium through the patterned growth of cells in vitro[9], which enabled the first biophysical explanation of conduction block in the heart[10–13]. The field of biomicrofluidics exploded[14–16] in the late 1990s with the introduction of poly(dimethylsiloxane) (PDMS), which is an optically transparent, soft elastomer ideal for biological applications on the small scale. The concept of mimicking the organ-level function of human physiology or disease using cells inside a microfluidic chip was first published in 2004, when Michael Shuler and colleagues first demonstrated a cell culture analogue (CCA) system that captured the systemic interaction between lung and liver on a one square inch silicon chip[17,18]. This system in conjunction with a physiologically based pharmacokinetic (PBPK) model has the potential to supplement animal studies and serve as a human surrogate for the prediction of clinical outcomes. A range of microfluidic devices have since been developed, mimicking diverse biological functions by culturing cells from blood vessels[19], muscles[20], bones[21], airways[22], liver[23,24], brain[25], gut[26,27] and kidney[28]. In 2010, the term organ-on-a-chip was invented by Donald Ingber, who developed a microfluidic chip to capture organ-level functions of the human lung[29]. Through the convergence of tissue engineering and microfluidics, miniature 3D models (also known as organs-on-a-chip) of various organs

[1]*Institute for Biomaterials and Biomedical Engineering, University of Toronto, Toronto, Ontario, Canada.*

[2]*Department of Chemical Engineering and Applied Chemistry, University of Toronto, Toronto, Ontario, Canada.*

[3]*Toronto General Research Institute, University Health Network, Toronto, Ontario, Canada.*

[4]*The Heart and Stroke/Richard Lewar Centre of Excellence, Toronto, Ontario, Canada.*

**e-mail: m.radisic@utoronto.ca*

https://doi.org/10.1038/s41578-018-0034-7

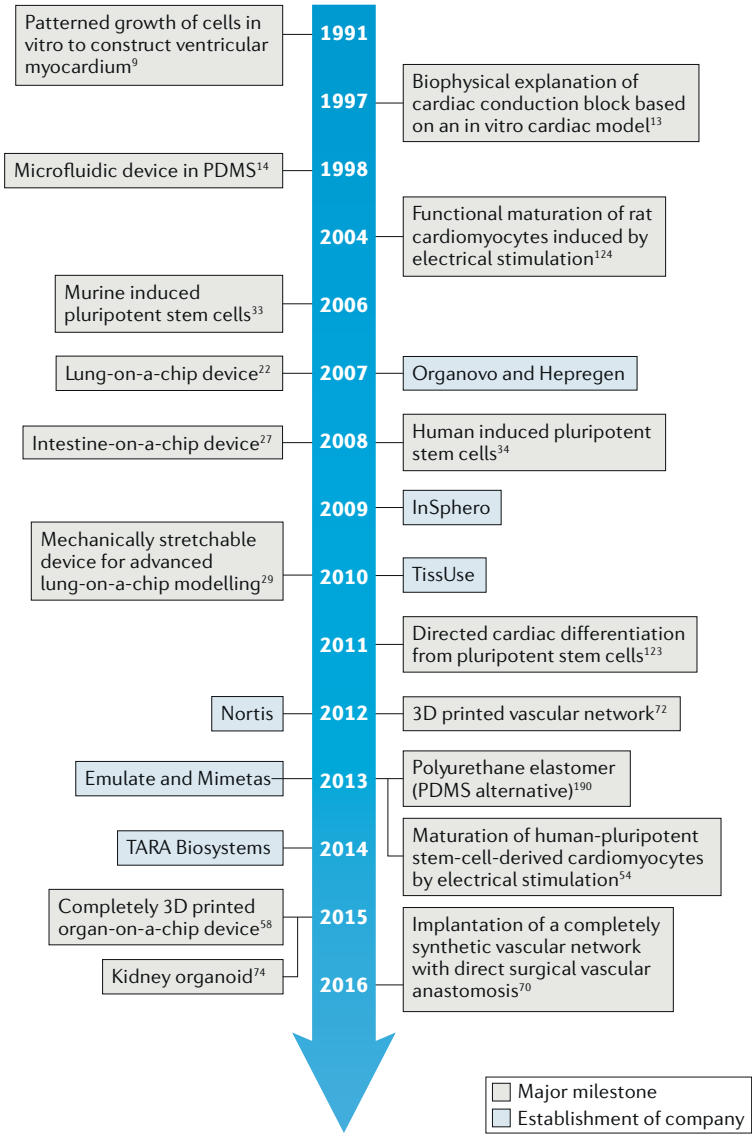

Fig. 1 | **Major milestones in organ-on-a-chip technology and establishment of organ-on-a-chip companies.** PDMS, poly(dimethylsiloxane).

have been engineered with the potential to transform the drug discovery industry[30] (FIG. 1).

The field of organs-on-a-chip is based on technological advances in tissue engineering and microfluidics as well as insights into the extraction, culture and maturation of human cells[31], enabling the design of customized cellular microenvironments with precise fluidic, mechanical and structural control[32]. A better understanding of pluripotent stem cell biology[33,34] has further enabled the cultivation and expansion of clinically relevant, patient-specific human cells. Organ-on-a-chip technology combines these aspects to reproduce key features of specific tissue microenvironments and architectures within a microfabricated device, facilitating the creation of 3D models that exhibit functional hallmarks of native tissues (for example, contractile properties and albumin secretion). The more precise the re-creation of the species-specific biology is, the better the predictive power of the in vitro model, which is at the heart of drug discovery.

Organ-on-a-chip engineering has attracted enormous interest and attention from the pharmaceutical industry, regulatory agencies and even national defence agencies[35], as also demonstrated by the emergence of at least 28 organ-on-a-chip companies in less than 7 years[36]. The primary focus of organ-on-a-chip technology is the re-creation of three key aspects of human physiology: the multicellular vascular or epithelial interfaces of organs (for example, blood vessel networks, lung and gut)[29,37–48], which function as barriers in tissues; the tissue-level organization of parenchymal cells (for example, liver, heart, skeletal muscle and tumours)[49–61], which are responsible for the key functional properties of an organ; and the systematic interaction of multiple organs (for example, drug absorption, distribution, metabolism and elimination involving the gut, circulation, liver and kidney)[62–69].

Advanced biofabrication techniques, such as 3D printing and 3D microfabrication can also be applied for the creation of tissue models, and organoid technologies can explore stem cells for the formation of organ-like structures to accurately and simultaneously capture multiple aspects of human physiology[70–73]. However, organ-on-a-chip technology not only incorporates multiple cell types but also involves engineering aspects, such as the guided spatial confinement of cells or the incorporation of sensors and microfluidic channels (BOX 1). By contrast, organoid approaches rely solely on the spontaneous self-assembly of cells to achieve complex tissue and organ-level organization and function[74]. There is certainly potential to merge these fields through synergistic engineering[75].

In this Review, we discuss organ-on-a-chip technology for its potential to reproduce tissue barriers, parenchymal tissues and inter-organ interactions and examine commercialization opportunities. We highlight representative physiological hallmarks realized in organ-on-a-chip devices and investigate how organ-on-a-chip technology can be useful for biological discovery. The success of this technology depends not only on its scientific validity but also on its usability, appropriate cell sources, cost of adoption and market size. Thus, we analyse the challenges in material selection[76], cellular fidelity[75], multiplexing and fluid handling[77], online readouts[69,78], scalable production[45], biological validation and integration into the existing drug development pipeline.

Reproducing tissue barrier function

In traditional drug screening approaches, organ-specific effects and the toxicity of a drug are examined using a homogeneous population of specific cells. However, human tissues and organs are not made of a homogeneous cell population. The complexity of human organs is based on intricate interactions between various specialized cell types arranged in precise geometries and interacting with specific microenvironments. These interactions often occur at well-defined tissue interfaces, enabling organ function (FIG. 2; TABLES 1,2).

Box 1 | **Organ-on-a-chip systems**

An organ-on-a-chip device typically contains one or several of the following components.

Geometrical confinement and patterning (see the figure, part a)

- Spatially defined multicellular co-culture
- Phenotypical change is induced by physical confinement

Presence of flow (see the figure, part b)

- Fluid inlets and outlets
- Physiological cell:liquid ratio

Environmental control (see the figure, part c)

- Mechanical stimulation and actuation
- Electrical stimulation
- Environmental control of O_2, CO_2, pH, nutrients and growth factors
- On-demand presence of drugs or toxins

Sensors and physiological readouts (see the figure, part d)

- Built-in electrodes
- Optical readouts
- Online sensors for biochemical readouts

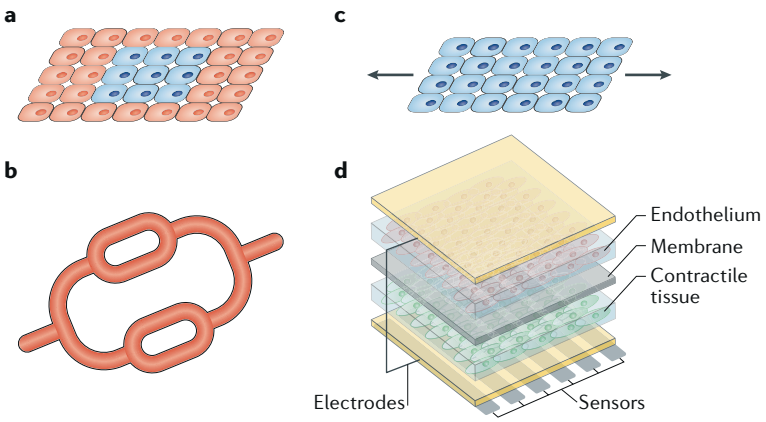

Figure adapted with permission from REF.[78], RSC.

Microfluidic membrane. Plastic membranes can be incorporated into microfluidic channels to model the barriers and interfaces of human tissues, such as the lung[22], intestine[27] and brain[25]. For example, a microfluidic device incorporating a mechanically stretchable membrane can capture the organ-level function of vascular and epithelial interfaces[29,39–42,79–84] (FIG. 2a). This device can be used to model the alveolar–capillary interface of the human lung by co-culturing microvascular endothelial cells and alveolar epithelial cells on a 10-μm-thin PDMS membrane. In addition to reproducing the structure of the tissue interface, vascular perfusion and breathing can be modelled within this device by applying cyclic mechanical strains[29], which can be explored for investigation of the inflammatory response to materials. For example, compared with animal tests, the application of cyclic strain more accurately accentuates the pulmonary inflammatory response to silica nanoparticles and the disruption of barrier function in response to interleukin-2 (IL-2)[29,80]. By adjusting the channel dimensions and using gut-specific cells, this platform can also model the human gut, in which cyclic strain induces the development of polarized columnar epithelium from human intestinal epithelial cells. The continuous perfusion along the epithelial compartment further enables long-term co-culture of an intestinal microorganism (*Lactobacillus rhamnosus* GG)[40,83] and modelling of an enterovirus infection[84]. Therefore, this device is ideal for the modelling of organ interfaces, at which cyclic strain and perfusion play a dominant role. This platform can be further adapted to recreate human kidney proximal tubules[39,85], kidney glomerulus[42], lung airway[41,86,87] and placenta[88], enabling fluid perfusion and biologically relevant molecular transport of key biochemical signals across tissue (TABLE 1) and vascular barriers (TABLE 2). Implementing pathological factors in these devices also allows for the modelling of human diseases, such as enterovirus infection of the human gut[84], effects of smoking on the lung airway[82] and breast ductal carcinoma[89].

Organ-on-a-chip devices benefit from the possibility to readily include dynamic environmental factors, improving cellular fidelity, and from compatibility with imaging. Complex biological events, such as neutrophil infiltration across the vascular barrier and pulmonary leakage, can be easily visualized and quantified, enabling a detailed investigation of the mechanism of action of specific drugs or environmental insults. Various PDMS-membrane-based devices are currently being commercialized by Emulate[90,91], originally derived from work conducted at the Wyss Institute for Biologically Inspired Engineering at Harvard. According to publicly available information, the company closed its series B venture with a total of US$45 million in investment and is poised to disrupt the global pharmaceutical research and development (R&D) market, which was estimated to be $141 billion in 2015 (REF.[92]), demonstrating that a small improvement in the efficiency of drug discovery could lead to billion-dollar savings for large pharmaceutical companies.

Microfluidic scaffolds. A standalone microfluidic network can be fabricated using a synthetic polymeric elastomer serving as a scaffold for the construction of vascularized functional tissues[70] (FIG. 2b). The microchannels defined by thin channel walls can be rendered permeable through the incorporation of microporosity and nanoporosity. The network maintains its mechanical stability, supporting endothelialization and culture of a surrounding dense parenchymal tissue. Using this approach, vascular interfaces of arbitrary dimensions can be established between endothelial cells and parenchymal tissues. For example, functional liver and cardiac tissue can be grown and tested with common drugs, which are perfused through the built-in internal vasculature. Such engineered cardiac tissues display macroscopic contraction, with the entire tissue being compressed at each contraction without collapse of the internal vasculature. The whole tissue can also be removed from the bioreactor and implanted in animals with direct surgical vascular connections, thus establishing immediate blood perfusion. This perfusable implantable chip, if populated with human cells, could potentially help bridge the gap between in vitro organ-on-a-chip testing and in vivo animal tests.

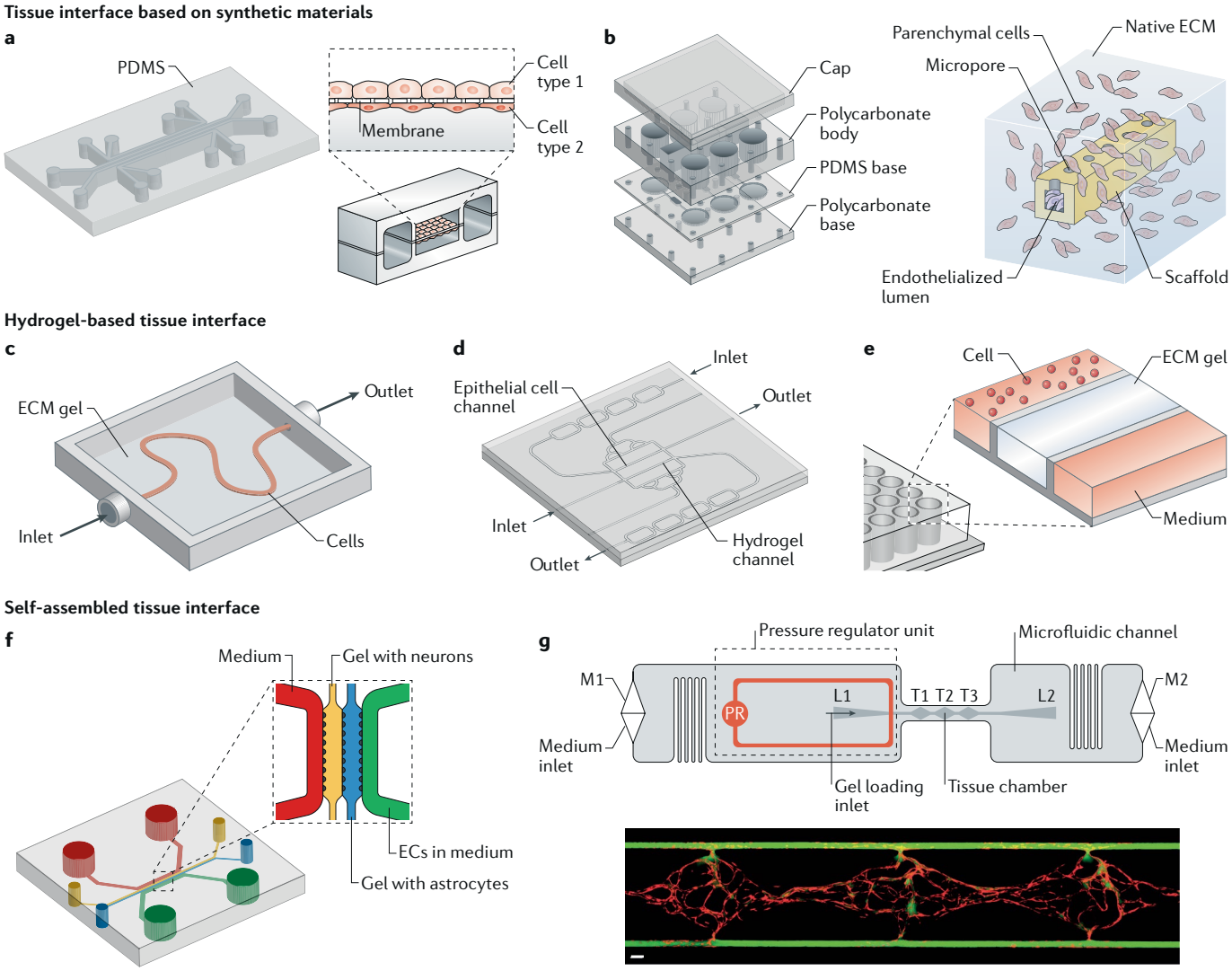

Fig. 2 | **Reproducing tissue barrier function.** Organ-on-a-chip devices can model biological tissue barriers using flexible and porous poly(dimethylsiloxane) (PDMS) membranes (panel **a**), perfusion bioreactors and synthetic microfabricated scaffolds (panel **b**), 3D printing of hydrogels (panel **c**), moulded hydrogels (panel **d**), phase-guided hydrogels (panel **e**), pro-angiogenic factor and flow-driven cellular self-assembly (panel **f**) and perfusion-driven vasculogenesis (panel **g**). The unit (panel **g**) contains three tissue chambers (T1–T3) connected to two microfluidic channels, two gel loading ports (L1 and L2), two medium ports (M1 and M2) and one pressure regulator (PR). The micrograph shows the formation of a vascular network within one tissue unit. Endothelial cells are shown in red; fluorescein isothiocyanate-labelled dextran (green) perfuses the vasculature. Scale bar = 100 µm. EC, endothelial cell; ECM, extracellular matrix. Panel **a** is adapted with permission from REF.[29], AAAS. Panel **b** is adapted from REF.[70], Macmillan Publishers Limited. Panel **c** is adapted from REF.[47], CC-BY-4.0. Panel **d** is adapted with permission from REF.[48], Elsevier. Panel **e** is adapted from REF.[45], CC-BY-4.0. Panel **f** is adapted with permission from REF.[43], RSC. Panel **g** is adapted with permission from REF.[115], RSC.

Microfluidic hydrogels. Microfluidic hydrogels, referring to hydrogels with built-in microchannels, offer an alternative method to model tissue interfaces. Hydrogels, such as collagen, Matrigel, gelatin and fibrin that contain 90 to 99% water, are highly permeable to biomolecules and therefore mitigate the need for incorporating micropores to improve material permeability, as is the case for PDMS-membrane-based devices or polymer-based devices[93]. For example, the diffusion coefficient of bovine serum albumin (BSA) in water (9.14×10^{-7} cm^2 s^{-1}) is very similar to the diffusivity of BSA in the hydrogel glycidyl methacrylate–hyaluronic acid (4.54×10^{-7} cm^2 s^{-1})[94]. However, the fragile material properties of hydrogels make it challenging to shape them into stable structures with a defined vascular–epithelial interface. Microfabrication and 3D printing of sacrificial materials can be applied to address this issue. Microfabricated microfluidic hydrogels can be prepared with complex microchannel networks and populated with various types of endothelial cells to create organ-specific vascular networks[38,95]. 3D printing further enables the creation of sophisticated channels, for example, of convoluted renal proximal tubules[47], and thus printing of an entire kidney might be possible in the near future (FIG. 2c). In contrast to modelling the tissue interface as a 2D membrane, the inherent

Table 1 | **Representative organ-specific epithelial barriers reproduced in organ-on-a-chip devices**

Cell sources	Functional hallmarks	Disease models and drug tests	Refs
Lung			
• Human alveolar epithelial cells and microvascular endothelial cells • Human type II alveolar epithelial-like A549 cells • Bronchial epithelial cells (16HBE14o) and primary HUVECs	• Formation of alveolar–capillary barrier and cell-modulated permeability • Presence of intercellular junction proteins (occludin and VE-cadherin) • Presence of air–liquid interface and fluid flow • Reproduction of breathing using cyclic mechanical strain • Intracellular production of ROS in response to nanoparticles	• Epithelial stimulation with inflammatory cytokine (TNF-α) • *Escherichia coli* infection • Infiltration of circulating neutrophils • Pulmonary toxicology of silica nanoparticles • IL-2-induced pulmonary oedema detected by fluid leakage across the air–liquid barrier	29,80,97
Small airway			
• Primary human AECs and primary human lung microvascular endothelial cells • Primary human AECs from individuals with chronic obstructive pulmonary disease	• Formation of airway barrier and cell-modulated permeability • Presence of continuous tight junction connections (ZO1, PECAM1, E-selectin, VCAM1 and ICAM1) • Formation of air–liquid interface and fluid flow • Presence of cilia and cilia beating • Cytokine secretion (IL-8, CCL2, CXCL1, IL-6, GM-CSF, M-CSF, CXCL10 and CCL5)	• Smoke-induced pathophysiology • Asthma (goblet cell hyperplasia, cytokine hypersecretion and decreased ciliary function) induced by IL-13 • Viral and bacterial infections with viral mimic poly(I:C) or LPS endotoxin • Therapeutic modulation of inflammatory cytokine and chemokine production with budesonide and BRD4 inhibitor • Enterovirus infection (coxsackievirus B1)	41,82
Gut			
Human intestinal epithelial cells (Caco-2)	• Formation of intestinal barrier function; molecular-mass-dependent permeability • Formation of tubular structure • Reproduction of gut movement using cyclic mechanical strain • Presence of intercellular junction proteins (occludin and ZO1) • Expression of glucose transporter (GLUT2), MRP2 transporters and ERBB1 and ERBB2 receptors • Formation of columnar villi with structural polarity and apical brush border (F-actin and ezrin) • Microbial co-culture (*Lactobacillus rhamnosus* GG) • Presence of catalytic activity (brush border aminopeptidase activity) • Polarized cytokine release (IP-10, IL-1β, IL-6, IL-8 and TNF-α) after injury	• Coxsackie B1 virus infected epithelium • Pathogenic bacteria (*Escherichia coli* or LPS endotoxin) induced injury • Bacterial overgrowth by cessation of peristalsis-like mechanical deformations • Loss of barrier function induced by staurosporine and aspirin	40,45,83,84
Kidney proximal tubules			
• Primary human PTECs • Human immortalized PTECs (RPTEC/TERT1 and ATCC CRL-4031)	• Formation of proximal tubule barrier • Formation of tubular or convoluted tubular structures • Separation of tubular flow and interstitial fluid • Presence of intercellular junction proteins (ZO1, CD13, E-cadherin and N-cadherin) • Polarization of epithelium (apical localization of ZO1 and basolateral distribution of Na/K-ATPase) • Presence of primary cilia (acetylated tubulin) • Presence of basolateral interdigitations and circular invaginations in the basement membrane • Cellular deposition of laminin and collagen type IV forming a basement membrane • Formation of columnar cell morphology and AQP1 expression • Shear-stress-induced production of SGLT2, α-tubulin, Na/K-ATPase and AQP1 proteins • High level of albumin uptake, cellular alkaline phosphatase activity and glucose uptake • Shear-dependent effects on Pgp transporter activity • Apical localization of γ-glutamyl transpeptidase and inhibition by acivicin • Glucose uptake inhibited by apigenin and dapagliflozin • ATP generation from mitochondrial oxidative phosphorylation as opposed to aerobic glycolysis • Transepithelial transport of para-aminohippurate • Indoxyl sulfate secretion, which is inhibited by probenecid • Para-aminohippurate secretion induced by indoxyl sulfate • Upregulation of HO1 and KIM1 under $CdCl_2$ treatment	• Cellular injury caused by basolateral application of cisplatin and subsequent recovery • Cyclosporine A-induced cytotoxicity	39,46–48

Table 1 (cont.) | **Representative organ-specific epithelial barriers reproduced in organ-on-a-chip devices**

Cell sources	Functional hallmarks	Disease models and drug tests	Refs
Kidney glomerulus			
• Human-iPSC-derived podocytes and human glomerular microvascular endothelial cells • Human immortalized podocytes • Murine glomerular endothelial cells and murine podocytes (MPC-5) • Primary glomeruli isolated from the renal cortices of 4-week-old rats	• Formation of glomerulus barrier and modulated permeability for large (albumin) and small (inulin) model proteins • Presence of fluid flow and mechanical strain • Presence of structural proteins (PAX2, WT1, nephrin, podocin, F-actin, synaptopodin, ZO1 and vimentin) • Expression and phosphorylation of PKCλ/ι, which potentially transports nephrin to the cell surface • Presence of primary and secondary cell foot processes • Molecular uptake of exogenous albumin • BSA filtration • Expression of FcRn (a receptor for albumin and IgG transport) and GLUT-1 (glucose transport protein) • Increased ratio of cytoplasmic to nuclear nephrin under mechanical strain • Urinary clearance of albumin and inulin molecules • Production and distribution of collagen type IV forming a basement membrane • ROS production in response to high glucose concentration	• Adriamycin-induced glomerular injury • Hypertensive nephropathy with increased perfusion rate • Filtration dysfunction under high glucose conditions	42,258,259
Placenta			
• BeWo b30 human trophoblast cell line and human primary placental villous endothelial cells • Human trophoblasts and HUVECs	• Formation of placenta barrier and cell-modulated permeability for large proteins • Compartmentalized fetal and maternal chambers with fluid flow • Expression of structural proteins (E-cadherin) • Cellular deposition of laminin forming a basement membrane • Formation of widespread microvilli on the apical cell surface (F-actin) • Trophoblast syncytialization in response to forskolin treatment shown by the reduction of barrier permeability and E-cadherin expression • Elevated β-human chorionic gonadotropin secretion in response to forskolin treatment • Expression and localization of GLUT1 transporters at apical membrane • Glucose transfer to fetal compartments	None	88,260

AECs, airway epithelial cells; AQP1, aquaporin 1; BRD4, bromodomain-containing protein 4; BSA, bovine serum albumin; CCL, CC-chemokine ligand; CXCL, CXC-chemokine ligand; FcRn, neonatal Fc receptor; GLUT1, glucose transporter 1; GM-CSF, granulocyte–macrophage colony-stimulating factor; HO1, haem oxygenase 1; HUVEC, human umbilical cord vein endothelial cell; ICAM1, intercellular adhesion molecule 1; IgG, immunoglobulin G; IL, interleukin; iPSC, induced pluripotent stem cell; KIM1, kidney injury molecule 1; LPS, lipopolysaccharide; M-CSF, macrophage colony-stimulating factor; PAX2, paired box 2; PECAM1, platelet endothelial cell adhesion molecule; Pgp, permeability glycoprotein; PKC, protein kinase C; poly(I:C), polyinosinic-polycytidylic acid; PTECs, proximal tubular epithelial cells; ROS, reactive oxygen species; SGLT2, sodium glucose cotransporter 2; TNF, tumour necrosis factor; VCAM1, vascular cell adhesion protein 1; VE-cadherin, vascular endothelial cadherin; WT1, Wilms tumour 1; ZO1, zonula occludens protein 1.

three-dimensionality of these hydrogel-based systems allows for the investigation of the 3D vascular–epithelial interface architecture and its impact on cellular and tissue functions, for example, how vessel architecture affects thrombus formation[37]. Nortis Bio, spun off from Washington University, is actively commercializing similar microfluidic devices with a tubular microchannel embedded inside a hydrogel as vascular and kidney models[46,48,96] (FIG. 2d).

Organs-on-a-plate. Membrane-based and hydrogel-based organ-on-a-chip devices can reproduce tissue barrier function; however, their commercial use is challenging owing to the fact that most conventional biological assays rely on multiwell plates and multichannel pipetting for liquid handling, but both of these approaches need a closed fluid circuit that requires external pumps for fluid control. Operating these devices requires specialized expertise, hampering their clinical translation. To transform membrane-based microfluidic devices to an open multiwell design, pneumatic deflection of a membrane suspended in an open well can be used to apply mechanical strain on the tissue barrier[97]. This system, commercialized by Alveolix, can be integrated with a microimpedance tomography (MITO) system for continuous monitoring of barrier permeability and mechanical strains[98]. Microfluidic hydrogel devices can also be adapted to a multiwell plate format by applying a phase guide principle to control the patterning of hydrogels using a simple pipetting technique, thus establishing a hydrogel–liquid interface at which the tissue barrier can be assembled in a multiwell plate (FIG. 2e). This system was pioneered by Mimetas. Furthermore, gravity-driven flow can be used to perfuse the system by simply tilting the platform, which not only eliminates the use of external pumps but also expands the platform to a 384-well plate format. Using this approach, Mimetas demonstrated the 3D culture of endothelium, intestinal epithelium and neuroepithelial-stem-cell-derived neurons[45,99–101].

Self-assembled microvasculature. In contrast to artificially defining the vascular–epithelial interface, growth factors and biochemical signals can be used to trigger the self-assembly of endothelial cells into a perfusable microvascular network within a hydrogel. Upon establishing proper connections to microchannels, such a self-assembled microvasculature can be perfused with a microfluidic circuit[102,103]. A variety of designs are available to improve vascular anastomosis with

Table 2 | **Representative organ-specific vascular and lymphatic barriers reproduced in organ-on-a-chip devices**

Cell sources	Functional hallmarks	Disease models and drug tests	Refs
Blood–brain barrier			
• Primary neurons, astrocytes and endothelial cells (HUVECs and hCMEC/D3) • Brain endothelial cells (b.End3) and astrocytes (C8D1A) • Primary human-brain-derived microvascular endothelial cells, pericytes and astrocytes • Neonatal rat brain capillary endothelial cells and neonatal rat astrocytes from the cerebral cortex of 2-week-old Sprague Dawley rats	• Formation of blood–brain barrier in the presence of astrocytes and neurons and cell-modulated permeability • Formation of tubular vessels • Presence of structural proteins (DCX, GFAP, ZO1, F-actin and VE-cadherin) • Reduced glutamate transport across the blood–brain barrier under flow • Neurite formation from neurons • Dose-dependent transient increase in permeability in response to histamine	Inflammation in response to lipopolysaccharide endotoxin or a cytokine cocktail of TNF-α, IL-1β, CCL2 and CCL8	43,261–264
Blood–retina barrier			
HUVECs, primary human lung fibroblasts and human retinal pigment epithelial cell line (ARPE-19 (ATCC))	• Formation of retinal pigment epithelium–choroid structure • Presence of structural proteins (F-actin, CD31, claudin 5 and ZO1) • Cellular deposition of laminin and collagen IV forming a basement membrane • Choroidal neovascularization in response to VEGF gradient	Bevacizumab inhibited angiogenic sprouting	265
Microvascular networks			
• Human endothelial colony-forming cell-derived endothelial cells isolated from cord blood and human normal lung fibroblasts • Human dermal microvascular endothelial cells • Human kidney peritubular microvascular endothelial cells • HUVECs	• Formation of vascular barrier with perivascular interaction • Vascular sprouting, self-assembly and perfusion • Presence of structural proteins (VE-cadherin, CD31, ZO1, F-actin and β-catenin) • Cellular deposition of laminin and collagen IV forming a basement membrane • Changes in F-actin distribution in response to luminal flow • Assembly of vWF fibres induced by fluid flow • Interstitial flow modulated endothelial sprouting, delocalization of VE-cadherin, redistribution of cortical actin and remodelling of cell–cell junctions • Endothelial migration in response to paracrine signalling and VEGF gradient • Fenestration in kidney peritubular micro-vessels (expression of PLVAP)	• Elevated gene expression of VCAM1, E-selectin, and ICAM1 in response to TNF-α • Increased leukocyte recruitment in response to TNF-α • Reduced vascular sprouting in response to treatment with inhibitors of Rho kinase (Y27633), tyrosine phosphorylation (Genistein), SRC kinase (PP2) and nitric oxide (L-NAME) and enzymes specific to heparan sulfate-cell glycocalyx component (Heparinase III) • Differential inhibition of angiogenesis by axitinib and glycolysis inhibitor (3PO)	37,38,70,72,95,103,105, 113–115,266–274
Artery			
Cerebral olfactory arteries isolated from C57BL/6 mice	• Vascular interface with circumferentially aligned smooth muscle cells • Presence of structural protein (F-actin) • Dynamic calcium response to phenylephrine treatment • Vessel dilatation in response to acetylcholine	Dose-dependent vasoconstriction in response to phenylephrine with and without nifedipine	275,276
Lymphatic vessels			
Primary human dermal lymphatic microvascular endothelial cells	• Formation of lymphatic barrier and cell-modulated permeability • Presence of structural proteins (F-actin, Podoplanin, PROX1, VE-cadherin, PECAM1 and ZO1) • Lymphangiogenesis in response to paracrine interactions with stromal fibroblasts • Lymphangiogenic sprouting in response to increasing gradient of pLFs, VEGF-A, VEGF-C, bFGF and S1P • Interstitial flow induced lymphatic sprouting • Enhanced PROX1 activity in response to interstitial flow • Reduced barrier permeability in response to cyclic AMP and phosphodiesterase inhibitor (Ro-20-1724)	Dose-dependent inhibition of lymphatic growth in response to FGFR1 and VEGFR2 inhibitor, SAR131675 VEGFR-3-TK inhibitor, cabozantinib, sunitinib, axitinib, FTY720(S)-P (S1PRs), W146 (S1P1R) and interferon-γ	121,277

bFGF, basic fibroblast growth factor; CCL, CC-chemokine ligand; DCX, doublecortin; FGFR1, fibroblast growth factor receptor 1; GFAP, glial fibrillary acidic protein; HUVEC, human umbilical cord vein endothelial cell; ICAM1, intercellular adhesion molecule 1; IL, interleukin; PECAM1, platelet endothelial cell adhesion molecule; pLFs, prolymphangiogenic factors; PLVAP, plasmalemmal vesicle-associated protein; PROX1, prospero homeobox 1; S1P, sphingosine-1-phosphate; TNF, tumour necrosis factor; VCAM1, vascular cell adhesion protein 1; VE-cadherin, vascular endothelial cadherin; VEGF, vascular endothelial growth factor; VEGFR2, vascular endothelial growth factor receptor 2; vWF, von Willebrand factor; ZO1, zonula occludens protein 1.

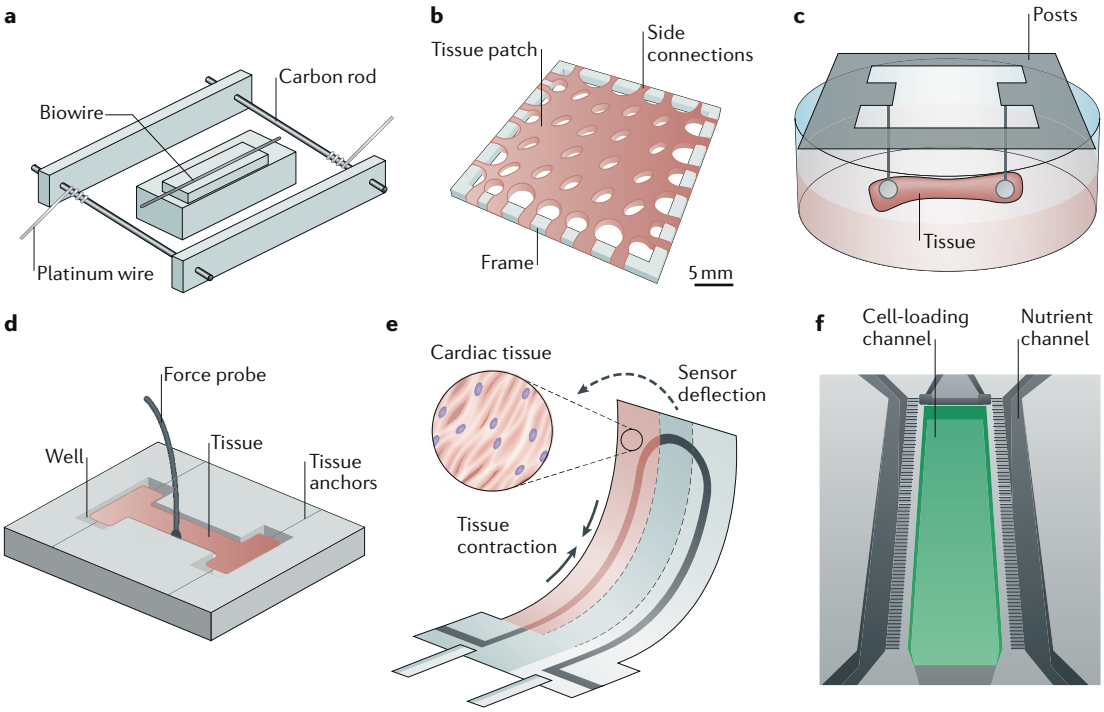

Fig. 3 | **Reproducing elongated parenchymal tissues.** Representative organ-on-a-chip devices that model the functions of elongated parenchymal tissues using different structural templates. Tissue can compact along microwires (panel **a**), posts can anchor a tissue network (panel **b**), tissues can hang on upside-down pillars (panel **c**), tissues can bridge across parallel rods (panel **d**), tissues can grow on flexible cantilevers (panel **e**) and tissue can grow along patterned channels and in grooves (panel **f**). Panel **a** is adapted with permission from REF.[256], Elsevier. Panel **b** is adapted with permission from REF.[130], Elsevier. Panel **c** is adapted from REF.[126], the publisher for this copyrighted material is Mary Ann Liebert, Inc. publishers. Panel **d** is adapted with permission from REF.[133], Elsevier. Panel **e** is adapted from REF.[58], Macmillan Publishers Limited. Panel **f** is adapted from REF.[55], CC-BY-4.0.

perfusable microfluidic channels, including multiple (FIG. 2f) or single (FIG. 2g) inlets and outlets[104–109]. Using this approach, micro-vessels can be engineered with vessel diameters close to the size of native capillaries (7–20 μm)[110]. Moreover, these microvascular networks are amenable to biological remodelling and thus vascular growth, deterioration and maturation in response to drugs and biochemical gradients can be monitored[111–114]. The devices are usually perfused with gravity-driven flow but can also be adapted to a multiwell plate format for easier use[115].

A horizontal compartmentalized layout further enables incorporation of multiple cell types in a spatially defined manner as well as monitoring of intercellular interactions using high-magnification imaging[116]. For example, in a blood–brain barrier model based on the co-culture of neurons, astrocytes and cerebral endothelial cells, the exact length and branching morphology of neurites can be traced and quantified over time[43]. Similarly, the entire process of cancer cell extravasation across the vascular barrier of microcapillaries can be imaged and tracked in models of tumour microenvironments[117,118]. Adjustment of the extracellular matrices and co-culture with cells of different organs cause breast cancer cells to exhibit organ-specific extravasation behaviour[44]. However, in these devices, the parenchymal space is inaccessible to users after formation. To overcome this limitation, the device can be transformed to an open-well design, in which preformed parenchymal tissues, such as tumour spheroids, can be placed on the preformed vascular bed in a multistep seeding approach, improving the versatility of this platform and allowing potential integration of the microvasculature with various models of dense solid tissues[119,120]. Most studies have focused on the vasculature and lymphangiogenesis[121] thus far, because of our in-depth understanding of the tubulogenesis process in these two organ systems. It remains to be seen if the same technology is adaptable to tubulogenesis of other organs that incorporate epithelial cells.

A variety of engineering methods have been developed to build tissue interfaces, and the ideal design will likely depend on the specific application and organ interface. Organ-on-a-chip systems are designed to validate specific drug targets and provide high-value data; however, the possibility of high-throughput screening using cells from a large population pool also needs to be considered in the device design. Biology is intrinsically variable, and to analyse subtle biological responses, data from an array of independent biological samples are required to capture unexpected drug toxicities in preclinical models.

Reproducing parenchymal tissue

If the epithelial–vascular interface is considered the door, then the parenchyma represents the house of a living tissue, because parenchymal cells enable the organ to function. In contrast to the tissue interface, parenchymal tissues have a 3D multicellular architecture, which is essential for their function (FIGS 3,4; TABLE 3).

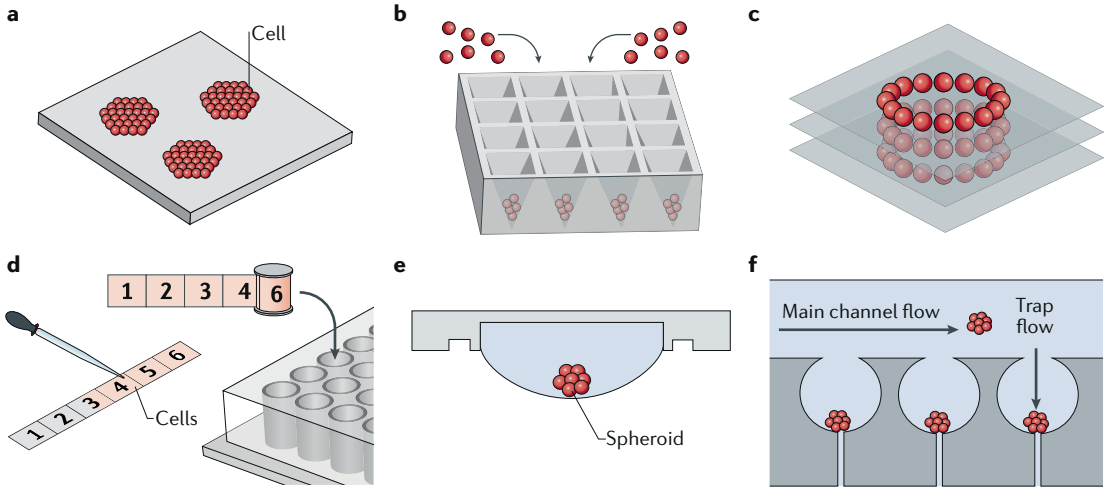

Fig. 4 | **Reproducing spherical parenchymal tissues.** Spherical parenchymal tissues can be generated and modelled by micropatterned clusters (panel **a**), inverted pyramidal wells (for self-aggregation) (panel **b**) and 3D multilayer bioprinting (panel **c**) or through rolled-up scaffolds that wind and unwind (panel **d**), hanging droplets (panel **e**) and microfluidic cell trapping (panel **f**). Panel **a** is adapted from REF.[50], Macmillan Publishers Limited. Panel **b** is adapted with permission from REF.[144], AAAS. Panel **c** is adapted with permission from REF.[257], IOP Publishing. Panel **d** is adapted from REF.[149], Macmillan Publishers Limited. Panel **e** is adapted from REF.[51], Macmillan Publishers Limited. Panel **f** is adapted with permission from REF.[175], RSC.

Parenchymal cells are densely packed and precisely organized to exhibit organ-specific functions.

Heart-on-a-chip. Cardiotoxicity is a major reason for drug recalls (Micturin, Fen-phen, Seldane, Vioxx and Avandia), and if discovered after preclinical and clinical studies, such drugs can cause lethal arrhythmias and death; for example, Vioxx has been linked to over 27,000 instances of heart attack and sudden cardiac death, costing Merck nearly $5 billion in criminal and civil settlements[122]. A major challenge for the development of suitable in vitro cardiac models for drug testing is the inability to obtain a sufficient number of cardiomyocytes from human hearts or to expand them in vitro owing to their limited proliferative capacity. Therefore, the pharmaceutical industry uses mathematical models and cell lines with overexpressed human ion channels (for example, the human ether-a-go-go-related gene potassium channel 1 (ERG; also known as KCNH2) in Chinese hamster ovary cells or human embryonic kidney cells), followed by tissue slices from animal hearts and in vivo studies in mice, rabbits or dogs to assess cardiotoxicity. The possibility to differentiate human induced pluripotent stem cells (iPSCs) and embryonic stem cells (ESCs) into large numbers of cardiomyocytes addresses the limitation of the lack of human cardiac cells[123]; however, many differentiation protocols result in cells that are structurally and functionally immature, resembling fetal rather than adult human cardiomyocytes, questioning their relevance for drug testing.

We have pioneered a system that uses electrical stimulation to improve the maturation of cardiac tissue in vitro, which is being commercialized by TARA Biosystems[54,124,125] (FIG. 3a). Engineered cardiac tissue that is stimulated by a dynamic electrical field of ramped-up frequency displays various hallmarks of maturation, such as improved myofibril organization, increased conduction velocity and cell size, and improved electrophysiology and Ca^{2+}-handling properties, compared with non-stimulated tissues. A similar degree of maturation can also be achieved using mechanical stimulation, because mechanical tension is essential for the elongation of cardiomyocytes and to establish aligned cardiac bundles in three dimensions[56,57,60,126–131] (FIG. 3b). Achieving adult-like maturation in engineered cardiac tissue is key for commercialization. Therefore, optimization of cell culture and protocols is required to generate mature cardiomyocytes with positive force–frequency relationships, post-stress potentiation, the presence of transverse tubules and highly organized mitochondria.

Methods are further required to readily probe tissue function in response to drug stimulation. In animal studies, changes in cardiomyocyte contraction are quantified by measuring ejection fraction, fractional shortening and systolic function. However, these data can be confounded by multiple parameters, such as changes in drug permeability, making it difficult to decouple the mechanisms of action. Various organ-on-a-chip platforms have been established to directly probe the contraction dynamics of engineered cardiac muscles. In the most widely used model, the cardiac tissue is wrapped around and suspended between two elastic posts (FIG. 3c). The passive and active bending of the posts is then correlated to the passive tension and the active force of tissue contraction. Alternatively, a cantilever-like device enables the measurement of cardiac contraction by optical detection[132]. An I-wire system can further be used to detect cardiac contraction using an external probe[59,133] (FIG. 3d). However, microscopic imaging or the use of expensive force probes does not allow high-throughput measurements to continuously and simultaneously track the functional changes of multiple tissues. To overcome this limitation, flexible cantilevers can be embedded with strain sensors to

Table 3 | **Representative organ-specific parenchymal tissues reproduced in organ-on-a-chip devices**

Cell sources	Functional hallmarks	Disease models and drug tests	Refs
Cardiac myocardium			
• Human-pluripotent-stem-cell-derived cardiomyocytes • Neonatal rat ventricular cells from 2-day-old neonatal Sprague Dawley rats	• Formation of aligned 3D tissue • Presence of structural proteins (α-actinin, F-actin, sarcomeric α-actinin, troponin T, Cx43, vimentin, heavy chain of myosin II, N-cadherin and desmoplakin) • Rod-like cellular shape • Lack of spontaneous contraction, low excitation threshold and high maximum capture rate in response to electrical stimulation • Presence of organized sarcomere structures (desmosomes, I bands and H zones) • Colocalization of T-tubules (caveolin 3) with Z-lines • Regularly distributed mitochondria • Presence of multinucleation, large sarcomere length and cell area • Localization of gap junctions to intercalated discs • Increase in Ca^{2+} transient in response to caffeine • Inhibition of L-type Ca^{2+} channels by verapamil or nifedipine and blockade of SERCA channels by thapsigargin • High level of ERG tail current density, I_{K1}, current density and cell capacitance • Low level of cell membrane potential • High level of conduction velocity and anisotropy in action potential propagation • Upregulation of sarcomere-associated genes (*MYL2*, *TNNI3*, *ACTN2*, *MYH7*, *MYL3*, *TNNC1*, *TNNT2*, *MYH11* and *SORBS1*), ion transporters and regulatory proteins • Chronotropic and inotropic response to β-adrenergic stimulation • Change in tissue elasticity in response to blebbistatin • High active force of contraction • Presence of tissue length–tension relationship that follows the Frank–Starling curve	• Drug-induced and stress-induced hypertrophy • Cardiac fibrosis • Chronic treatment with isoprenaline, angiotensin II or endothelin 1 • Arrhythmia with incomplete re-entrant wave-like system and defibrillation by electrical stimulation	54,57,59, 124,130, 278–282
Skeletal muscle			
• Motor neurons differentiated from mouse embryonic stem cell line HBG3 (Hb9-GFP) • Mouse myoblasts (C2C12) • Skeletal muscle dissected from the hindlimb of the rat fetus at embryonic day 18	• Formation of elongated 3D skeletal muscle • Presence of neuromuscular junction (myosin heavy chain and β-III tubulin) • Colocalization of nerve terminals (indicated by synaptophysin) and AchR (indicated by BTX-488) • Structural protein expression (α-actinin, F-actin and myogenin) • Delayed muscle stimulation in response to glutamate	None	132,229,283
Liver			
• Pluripotent-stem-cell-derived human hepatocytes and murine embryonic 3T3-J2 fibroblasts • Primary human hepatocytes • Immortalized hepatocyte cell line (HepG2) • Primary mouse, rat and dog hepatocytes	• Monolayer co-culture of stromal cells, Kupffer cells and stellate cells • 3D co-culture of stromal cells, Kupffer cells and stellate cells • Presence of structural proteins (ZO1 and E-cadherin) • Formation of bile canaliculi (MRP2) and transport of fluorometric dye • Cell polarity (basolateral marker CD26) • High level of urea and albumin production and secretion • High level of activities of phase I (CYP450) and phase II (conjugation) enzymes • Modulation of gluconeogenesis by prototypical hormones, insulin and glucagon • mRNA expression of key glucose metabolism genes (phosphoenolpyruvate carboxykinase 1) and phase I and II genes • Production of human-unique metabolites through CYP2C9, UGT1A4, aldehyde oxidase or N-acetyltransferase	• Drug toxicity screening with acetaminophen, amiodarone, benzbromarone, clozapine, diclofenac, flurbiprofen, mebendazole, mefenamic acid, phenacetin, phenylbutazone, quinine, trazodone HCl, troglitazone, aspirin, buspirone, dexamethasone, dextromethorphan HBr, fluoxetine, miconazole, prednisone, propranolol, rosiglitazone, warfarin, acetazolamide, betahistine 2HCl, captopril, chloramphenicol palmitate, ciprofloxacin HCl, clomiphene citrate, clomipramine, cyclophosphamide, cyproterone acetate, danazol, dapsone, estrone, hydroxyurea, imipramine HCl, isoniazid, maleic acid, methimazole, nifedipine, norgestrel, nortriptyline HCl, piroxicam, progesterone, pyrazinamide and tamoxifen • Inhibition of gluconeogenesis by metformin and 3-mercaptopicolinic acid • Hyperglycaemia-induced lipid accumulation	49,50, 53,70, 138–140, 143,148, 160,163, 284–286

Table 3 (cont.) | **Representative organ-specific parenchymal tissues reproduced in organ-on-a-chip devices**

Cell sources	Functional hallmarks	Disease models and drug tests	Refs
Liver (cont.)			
		• Hepatic clearance of warfarin, meloxicam, tolbutamide, diazepam, alprazolam, glimepiride, theophylline, prednisolone, riluzole, voriconazole, risperidone, flecainide, atomoxetine, diclofenac, atazanavir, midazolam and lidocaine • Hepatitis B and C virus infection • Pro-inflammatory cytokines associated infection and inflammation • Compound-induced fibrogenesis (methotrexate, thioacetamide and TGF-β1) • Trovafloxacin-induced dose-dependent toxicity	
Tumour			
• Breast cancer cells (MDA-MB-231, MCF-7, HTB-133 and MDA-MB-361) • Non-metastatic mammary epithelial cells (MCF-10 A) • Colorectal cancer cells (HCT116, SW620 and SW480) • Melanoma cell line (MNT-1) • Osteosarcoma (MG-63 cells, CRL1543 and ACC 243) • Lung adenocarcinoma cells (A549) • Ductal carcinoma in situ cell lines (DCIS)	• Formation of cancer spheroids integrated with perfusable microvasculature • Tumour extravasation and intravasation across vascular barrier • Macrophages and TNF-α-regulated cancer intravasation • Differential cancer cell extravasation rate in organ-specific microenvironments (for example, bone and muscle) • Changes in the rate of cancer cell extravasation induced by fluid flow • Inhibition of cancer extravasation by adenosine • Reduced tumour growth in response to chemotherapeutical drugs (vinblastine, docetaxel and doxorubicin) • Vinblastine-induced sensitization to radiation therapy • Presence of oxygen and biochemical gradient and induced differential response to doxorubicin and radiation therapy • Epithelial–mesenchymal transition accompanied by changes of vimentin and E-cadherin expression • Cancer growth inhibition by intravenous administration of paclitaxel	• Drug screening on tumour growth and associated vasculature (bortezomib, vincristine, mitomycin C, gemcitabine, vorinostat, tamoxifen, linifanib, axitinib and sorafenib, pazopanib, oxaliplatin, folinic acid (leucovorin) and 5-fluorouracil) • Inhibition of cancer dispersion and proliferation by kinase inhibitors	44,89, 112,115, 117,118, 287,288
Adipose tissue			
Murine 3T3-L1 pre-adipocyte-derived adipose cells	• Perfusable vascular and adipose tissue interface • Uptake of fatty acid	None	172
Peripheral nerve			
• Dorsal root ganglia cells from embryonic day 5–16 rats • Oligodendrocytes from newborn rat cerebral cortices • Low-density hippocampal cultures from embryonic day 18 rats • Rat cortical neurons from embryonic day 17–18 rat cortices • Human iPSC-derived neuroepithelial stem cells	• Compartmentalization of glial cells and neurites • Presence of structural proteins (axonal neurofilament-H, α-tubulin, actin, tau-1 and MAP2) • Myelination by Schwann cells (MBP) • Formation of nodes of Ranvier (localization of CASPR in the paranodal regions that flank the nodes of Ranvier) • Association of oligodendrocytes with multiple axons • Polarization of neuron growth • Compartmentalization of corticostriatal neuronal networks • Improved neurite outgrowth in response to treatment with ROCK inhibitor (Y27632); waveform properties characteristic of compound action potentials	• Elimination of field potential response by Na^+ channel blocker (tetrodotoxin) • Axonal degeneration after nerve compression • Axonal fragmentation induced by somatic Aβ peptide • Remote *trans*-synaptic alterations in response to somatic applications of β-amyloid peptides in corticostriatal neuronal networks	99,289–297

AChR, acetylcholine receptor; CASPR, contactin-associated protein 1; Cx43, connexin 43; CYP450, cytochrome P450; ERG, ether-a-go-go-related gene potassium channel 1; iPSC, induced pluripotent stem cell; MAP2, microtubule-associated protein 2; MBP, myelin basic protein; MRP2, multidrug resistance-associated protein 2; ROCK, Rho-associated protein kinase; SERCA, sarcoendoplasmic reticulum calcium transport ATPase; Tau-1, microtubule-associated protein tau; TGF, transforming growth factor; TNF, tumour necrosis factor; ZO1, zonula occludens protein 1.

electrically and simultaneously detect the contraction of multiple cardiac tissues[58] (FIG. 3e). This system is one of the first organ-on-a-chip devices that was completely manufactured by 3D printing[58].

These microscale organ-on-a-chip devices can also be scaled up for high-throughput measurements at lower cost and with fewer biological resources than systems that require a large amount of expensive media for the culture of cardiomyocytes derived from pluripotent stem cells. Furthermore, cardiac models based on microfluidics (FIG. 3f) reduce the number of cardiomyocytes from millions of cells to several thousand cells per tissue[55], compared with other macroscale systems. Given the high cost of cardiomyocytes, this reduction in cell number and reagents leads to considerable savings in the acquisition of experimental data.

Liver-on-a-chip. Liver toxicity is another major cause of drug recalls, making up 32% of all cases of post-approval drug withdrawals between 1975 and 2007 (REF.[134]) (for example, trovafloxacin[135]). The liver is the first organ that ingested drugs encounter after entering the bloodstream. In contrast to cardiomyocytes, hepatocytes, the metabolic engine of the liver, can proliferate and be obtained from human biopsies and thus there is no shortage of human hepatocyte cell sources. However, maintaining the functionality of hepatocytes in vitro can be challenging, because the liver-specific functions of hepatocytes, such as enzymatic activity and albumin secretion, rapidly deteriorate after removal from their native environment. Cell polarity, oxygen gradients, access to bile canaliculi and microvasculature are immediately lost after liver tissue dissociation. Therefore, metabolic function and enzymatic activity of hepatocytes substantially decrease within 1 week of in vitro culture.

Heterotypic (crosstalk between different cell types) and homotypic (crosstalk between the same cell type) interactions between hepatocytes and stromal cells are crucial for maintaining hepatocyte functions in vitro[49,50,136–140]. To investigate these cellular interactions, a micropatterning technique can be applied to deposit clusters of hepatocytes and stromal cells on a 2D surface. The balance of homotypic and heterotypic interactions can be fine-tuned by varying cluster size and separation distance to keep hepatocytes functional in culture for weeks[50]. This technology was commercialized as HepatoPac by Hepregen, which was later acquired by Ascendance Biotechnology (FIG. 4a). In a collaborative study with Pfizer[141], HepatoPac tested 45 drugs using chronic drug exposure over 14 days to assess drug toxicity with a 65% success rate, which is a significant improvement over conventional platforms[141,142]. However, the mechanisms of action of many drugs are modulated by inflammatory pathways. For example, a drug could indirectly affect liver cells by altering the secretion of histamine and cytokines from immune cells in the liver. Therefore, to improve the accuracy of toxicity screening, macrophage-like primary human Kupffer cells and hepatic stellate cells can be incorporated into the system to assess the effects of pro-inflammatory cytokines on liver toxicity[143].

Intaglio-Void/Embed-Relief Topographic (InVERT) moulding[138] enables the 3D micropatterning of tissue cultures and can be applied to pattern 3D aggregates of stromal cells and hepatocytes in a hydrogel (FIG. 4b). This hydrogel system shows good engraftment in mice and grows in size by 50-fold over 11 weeks, representing a substantial level of regeneration[144]. Organovo, a 3D bioprinting company, also builds 3D liver models for toxicity screening in collaboration with pharmaceutical companies (for example, GlaxoSmithKline, GSK). They apply 3D printing for cell patterning, which is especially useful for hepatocyte culture owing to the importance of heterotypic and homotypic cell interactions[53,145–148] and the spherical morphology of these cell clusters (FIG. 4c). Moreover, the tissues printed by Organovo are large in size; they can generate a disc-shaped tissue with a minimal thickness of 250 μm (REF.[53]), which is ideal for the modelling of biochemically induced liver fibrosis[148] and for assessment by histological sectioning, which is a standard technique used in the clinic to detect liver disease and drug toxicity. However, in a thick 3D tissue, chemical and oxygen gradients are formed, affecting cellular function and response. Rolled-up tumour tissue (tumour roll for analysis of cellular environment and response, TRACER) that can rapidly assemble and delaminate can be used to spatially resolve, quantify and analyse the effects of hypoxic gradients on cancer cell metabolism and phenotype[149] (FIG. 4d).

Hanging drop technology can be applied to create cell aggregates in suspension, which is a desirable microenvironment for liver, pancreas or tumour cells (FIG. 4e). This technology has been commercialized by inSphero[52,150–153] and 3D biomatrix[154,155]. Alternatively, microfluidic trap arrays can be used for high-throughput trapping and screening of hundreds of cell aggregates or even microorganisms[156–159] (FIG. 4f). Combined with microfluidic perfusion circuits, tissue aggregates can also be cultured in a perfusable microenvironment, in which multi-organ interactions can be readily established[52,152]. HμREL is one of first companies in the liver toxicity field. Some of their technologies that are currently being developed originated from Michael Shuler's early work on a microscale cell culture analogue (μCCA)[17,160–163], enabling perfusion culture of liver cells from human, dog and rat. The platform is particularly useful in predicting hepatic clearance using continuous recirculation of culture media over a hepatocyte monolayer[164].

Body-on-a-chip

Integrated systems with multiple microscale cellular environments can be designed to simulate the systematic function of the human body and to predict the pharmacokinetics (PK) of new drugs (FIG. 5). Body-on-a-chip devices coupled with PK models aim to mimic the physiological complexity of inter-organ interactions. For example, such systems could be used to assess how the human body absorbs, distributes, metabolizes and eliminates (known as ADME) drugs or how hormonal signalling is orchestrated across multiple organs. However, the challenge remains of how to replicate the proportional scaling of each organ to reflect physiologically relevant interactions[165,166]. Various physiological parameters, such as the surface area of tissue barriers, organ mass, blood residence time and variation in tissue metabolism and functionality,

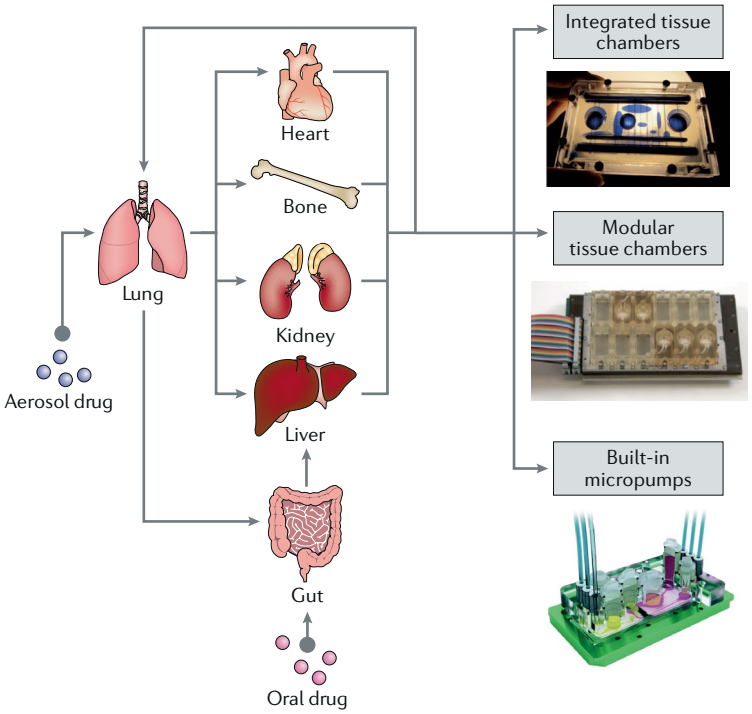

Fig. 5 | **Body-on-a-chip devices.** Organ-on-a-chip devices model the basic function of the tissue of a single organ. The integration of multiple such units can be used to model complex multi-organ interactions and higher-level systemic functions. Multi-organ body-on-a-chip devices can be engineered using integrated tissue chambers, modular tissue chambers and built-in micropumps.Integrated chambers image is reproduced with permission from REF.[62], Wiley. Modular chambers image is reproduced from REF.[67], CC-BY-3.0. Micro-pumps image is reproduced from REF.[64], CC-BY-4.0. Overview figure is adapted with permission from REF.[224], Cell Press.

need to be considered in the scaling process. However, the interplay of these factors in the body is still unknown for many organs. Body-on-a-chip devices in conjunction with computational modelling could potentially provide the necessary tools to gain insight into these interactions.

Inter-organ signalling. A microfluidic cell culture device based on 14 compartments representing 13 organs has been developed as a body-on-a-chip approach to model inter-organ crosstalk and to assess the relationship between organ volume and blood residence time[62] (FIG. 5). The organ models were categorized as barrier tissues and non-barrier tissues, and drugs were forced to first pass through the barrier tissues (skin, gastrointestinal (GI) tract and lung) before entering the fluid circulation and non-barrier tissues. Although only five cell lines were used, this proof-of-concept study demonstrated that cells can be kept viable for at least 1 week, which is remarkable given the complexity of the system. Alternatively, fewer organ models can be included to better characterize the interaction between different organs[63,167,168]. In these devices, fluid perfusion is achieved by gravity-driven flow, without the need for an external pump, simplifying the experimental setup[62,169]. Fluid circulation on a chip can also be realized with built-in micropumps. For example, TissUse developed a series of platforms equipped with built-in micropumps to maintain multiple distinct circulation systems (for example, surrogate blood flow circuit and an excretory flow circuit) separated by organ-specific epithelial cells cultured on plastic membranes[67,155,170]. These platforms can be used to model multi-organ interactions, specifically the ADME profile of drugs (FIG. 5). Similarly, a two-organ system, including pancreatic islets and liver spheroids, can be used to model the functional feedback loop of insulin secretion and glucose uptake between the pancreas and the liver. The experiments were conducted by two independent laboratories to establish robustness and reproducibility of the platform, which will allow researchers to model the pathogenesis of human type 2 diabetes mellitus[171]. However, white adipose tissue (WAT), which is an insulin-sensitive organ and an energy storage site that plays an important role in diabetes and affects the ADME profile of drugs through the sequestering of hydrophobic drugs, is not included in most multi-organ models. Owing to their fragility, buoyancy and transparent nature, the handling and culture of adipose cells within microfluidic devices are difficult. To overcome this challenge, a WAT-on-a-chip device prototype has been developed to culture and maintain adipose tissue that is able to uptake fatty acids after 2 weeks in culture[172]. The human reproductive tract and the 28-day menstrual cycle can be modelled by the co-culture of explanted mouse ovaries and human fallopian tube, uterus, cervix and liver[64] (FIG. 5). This modular platform allows for analysis of the effect of different hormonal profiles on the menstrual cycle. A body-on-a-chip system can also be built with each tissue model residing on a different chip. For example, a functional coupling approach can be used to integrate two or four different human microphysiological systems located at multiple different physical locations to study inter-organ effects of common drugs[66] (FIG. 6).

Incorporating quantitative systems pharmacology into body-on-a-chip systems is important to gain insight into the complex pharmacokinetics and biological interactions that arise from a multi-organ model. For example, a quantitative systems pharmacology approach can be applied to a perfused multiwell plate liver and immune model to measure the metabolism of hydrocortisone and the secretion of IL-6 and tumour necrosis factor (TNF)-α and to derive pharmacokinetic parameters. These parameters can then be implemented into a four-organ microphysiological system[173]. The integration of computational analysis and sufficiently complex microphysiological systems will certainly prove useful to better capture unanticipated actions of drugs[174]. Multi-organ systems can be augmented using other biofabrication techniques, such as hanging drop technology (FIG. 7a) or 3D printing (FIG. 7b), to improve the structural fidelity of modelled tissues. Using these technologies, the tissues can be first customized and then incorporated into a microfluidic system, which can be equipped with complex fluid circuits for automatic sampling and with built-in sensors for online readouts.

Inter-organ cell migration. Most multi-organ-on-a-chip systems focus on the modelling of biochemical signalling, and biochemical signals can be readily transported in the circulating fluid. However, only a few platforms have been developed to capture the inter-organ

trafficking of living cells. In the body, immune cells, white blood cells and cancer cells are transported in the circulation system across multiple organs, a key event in cancer metastasis. We developed a 96-well plate platform, called integrated vasculature for assessing dynamic events (InVADE), that can be integrated with multiple 3D vascularized tissues through a common built-in vasculature[175] (FIG. 7c). In this system, a continuous and short vascular connection between the different organs, with no dead volume, allows effective cell migration and transport. The multiwell plate platform further uses gravity-driven flow, is easy to use and enables modelling of the entire cancer metastasis cascade involving cancer cell extravasation from the tumour, transportation in the circulation and infiltration of a distant organ. HμREL in collaboration with L'Oreal is developing an Allergy Test-on-a-Chip device to model allergic reactions, which involve the migration of immune cells from the lymph node to the skin. This two-organ system contains two chambers, which are separated by an array of microfluidic channels, to maintain a chemical gradient across the organs. The chemical gradient drives the migration of immune cells, such as dendritic cells or T cells, from the lymph node compartment to the skin compartment, mimicking an allergic reaction[176].

Organ scaling in body-on-a-chip devices remains a challenge. However, the modelling of inter-organ biochemical crosstalk, of the ADME profile of drugs and of cellular trafficking across multiple organs is already possible with current platforms. The differences in the physiology of men and women further complicate the testing of disease mechanisms and drug efficacy using common in vitro and in vivo models; for example, treatment of pregnant women with the drug thalidomide, designed in the late 1950s to treat morning sickness, resulted in 10,000 severe birth defects[177], which could have been predicted using embryonic animal models[178]. Body-on-a-chip systems can be applied to model sex-specific hormonal levels and reproductive organs to correct the existing sex bias in clinical research and to gain a deeper understanding of the sex-specific mechanisms of drugs[179]. However, many proof-of-concept body-on-a-chip systems have used immortalized cell lines and primary animal cells that lack physiological relevance. Thus, validation experiments using relevant human cell types will be required to demonstrate the clinical applicability of these platforms.

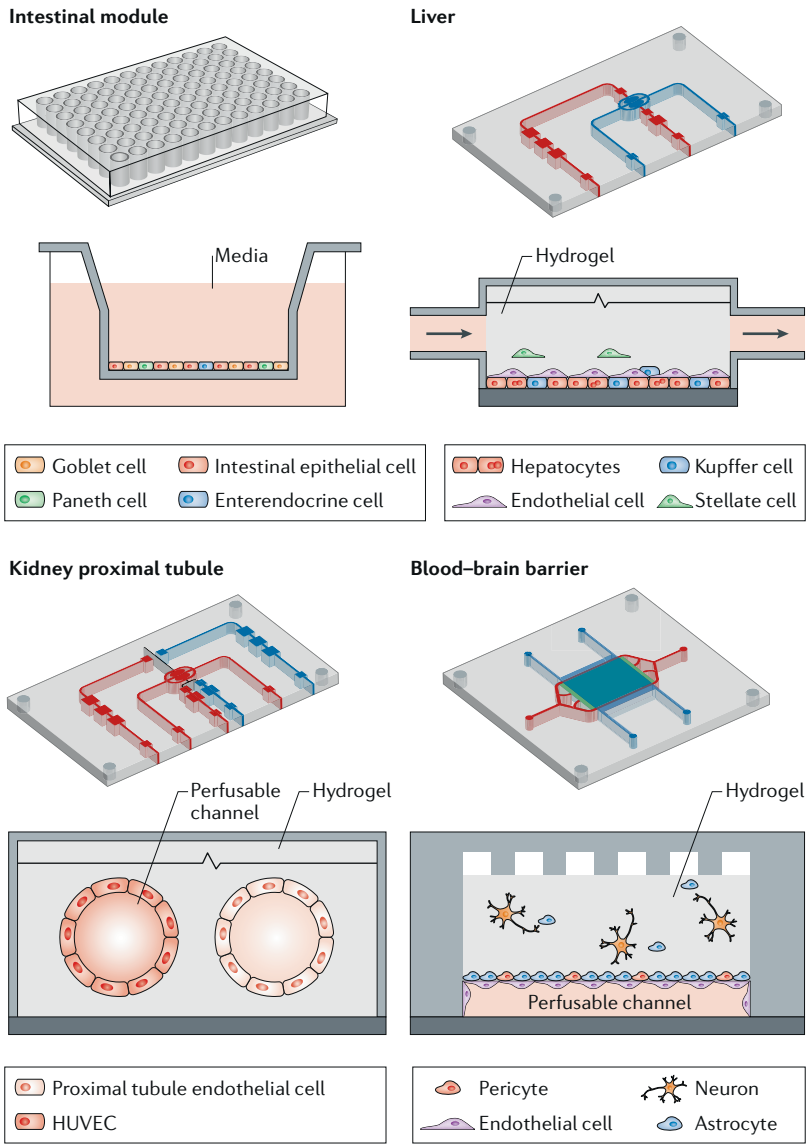

Fig. 6 | **Functional scaling of body-on-a-chip devices.** The connection of single organ units and combinations thereof into a larger body-on-a-chip device requires careful matching of organ-to-organ proportions, relevant functional models for accurate organ coupling and fluid transfer between compartments. Basolateral medium from the intestinal module is transferred into the liver module inlet. Outlet media from the liver are transferred to both the kidney proximal tubule compartment and the blood–brain barrier compartment. With each transfer, the media must be diluted and supplemented to suit the environment of the incoming organ. HUVEC, human umbilical cord vein endothelial cell. Figure adapted from REF.[66], CC-BY-4.0.

Challenges and outlook

Materials. Materials for organ-on-a-chip engineering need to be designed for both the engineering of the device and to support cell culture. Thus, one type of biomaterial needs to fulfil a range of requirements. PDMS has been the favourite material for the microfabrication-based rapid prototyping of devices owing to its advantages over standard polystyrene tissue culture plastic[76]. PDMS has an elastic modulus in the range of ~1–3 MPa and thus is highly compliant and deformable, making it applicable for replica moulding and microfluidic handling. PDMS can also be plasma functionalized to stack and bind multiple layers of PDMS together, enabling the fabrication of networks of microstructures[180]. For example, micromechanical devices can be built based on channels, pneumatic pumps and valves for micro total analysis 'lab-on-a-chip' systems[181,182]. Pneumatically controlled deformation across microchannels enables the programmed circulation of small quantities of reagents and fluids directly on the chip, allowing for the scale down of lab experiments, for example, for chemical analyses, cell capturing, transfection and immunoassays, by using multiplexed high-throughput patterning[183–185]. Similarly, the elastic deformation of PDMS can be used for the creation of biomimetic cell culture scaffolds, such as cyclically stretched lung-on-a-chip or other interfacial

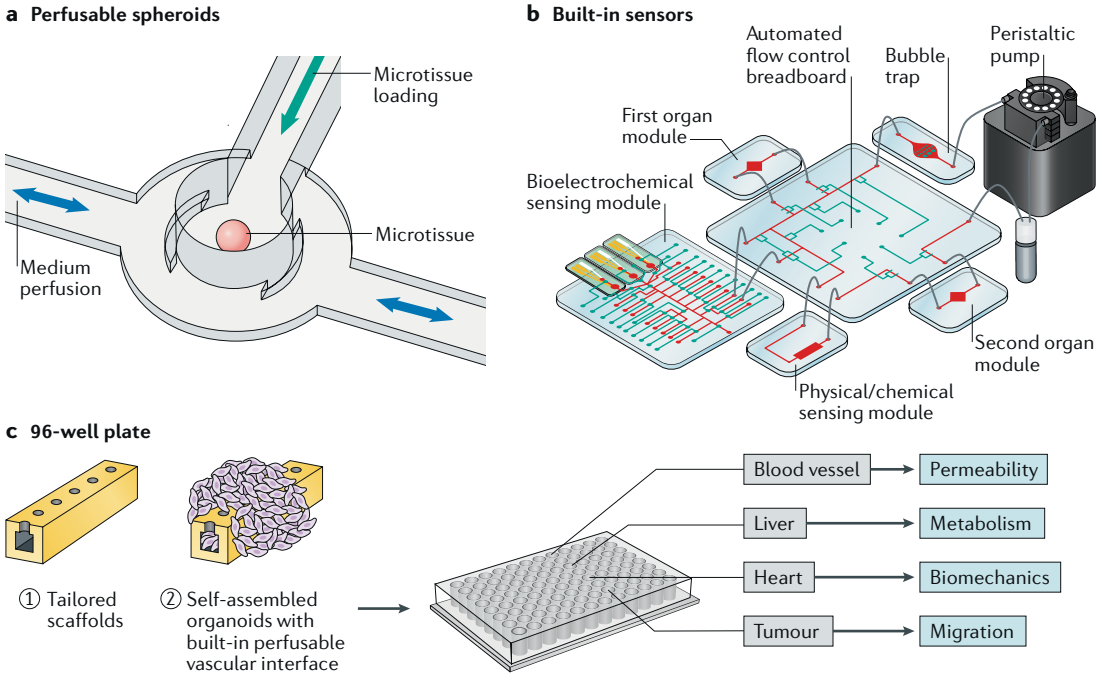

Fig. 7 | **Modelling multi-organ interactions.** Interactions between organs can be modelled using spheroids patterned within a perfusable microfluidic device (panel **a**), tissue modules integrated with built-in sensors for real-time interaction monitoring (panel **b**) or interconnected 96-well plate tissue chambers linked through long vascular conduits (panel **c**). Panel **a** is adapted with permission from REF.[152], Elsevier. Panel **b** is adapted with permission from REF.[69], Proceedings of the National Academy of Sciences. Panel **c** is adapted with permission from REF.[175], Wiley.

tissue-on-a-chip systems[29,42]. Bending of PDMS posts can further be applied to mechanically stimulate parenchymal cardiac tissue, inspired by the beating of the heart[186]. Moreover, PDMS is optically transparent and therefore accessible to optical microscopy to image fluid flow in the device. Finally, PDMS is biocompatible and oxygen permeable, making it suitable for biological experiments. However, the same material properties that are of advantage for microscale bioengineering also impart several challenges. For example, flexibility can lead to unwanted bulging and distortion if not carefully adjusted, gas permeability makes devices susceptible to medium evaporation and bubble formation, and PDMS absorbs and can subsequently leach out hydrophobic drugs and compounds in the culture medium[76]. These features compromise the consistency and accuracy of experiments, which is problematic owing to the small working volumes and high surface-to-volume ratio. Therefore, drug-inert polystyrene has been the standard material for cell culture for many decades, providing stability to reliably conduct biological experiments.

Many organ-on-a-chip companies that produce conventional multiwell plate formats are incorporating polystyrene (for example, Mimetas, AIM Biotech, InSphero and TARA Biosystems); however, in contrast to elastic PDMS, polystyrene is rigid. Therefore, new non-absorbent elastomeric materials need to be developed for applications that require an elastic material. Many new materials, such as styrene–ethylene/butylene–styrene and polyurethane elastomers[187–190], have already been developed specifically for organ-on-a-chip engineering, featuring properties such as castability, flexibility, optical transparency and non-absorption; however, they have not yet been widely adopted. Alternatively, coating technologies using parylene[191] or paraffin[192] can be applied to render PDMS non-absorbent, but they might negatively affect cell attachment. Hydrophilic materials, such as hydrogels[71] and polyesters[193,194], which are less drug-absorbent than PDMS, have also been used. Ultimately, the desired material properties will depend on the specific application, potentially shifting the industry towards a case-by-case approach regarding material selection. Alternatively, organ-on-a-chip devices could benefit from the integration of components made from multiple different materials to satisfy various design criteria simultaneously.

Cellular fidelity. The validity of a cell or tissue model strongly depends on the cells used to create it. Cells can be obtained from immortalized cell lines, ESCs, iPSCs or animal or human samples. Most organ-on-a-chip technologies have used cell lines to model human physiology thus far, especially for initial device validation. However, serial passaging of cells and genetic changes made to immortalize cell lines alter cell genotype and phenotype[195]. Stem-cell-derived progenitor or mature cells, especially cells derived from patients, provide greater clinical value and enable more accurate disease modelling than cell lines[196]. ESCs and iPSCs are highly proliferative and retain their pluripotent potential in culture; therefore, they can be differentiated into any desired cell type in vitro. Immature progeny derived from stem cells can be cultured in the specific microenvironments of organ-on-a-chip devices to induce their maturation[197]. Primary, mature cells certainly constitute

the most relevant cell type for the analysis and modelling of functional tissue models; however, primary cells are challenging to collect in sufficiently high numbers, and removal from their native environment often results in dedifferentiation and rapid functional decline, affecting their maturity[198].

iPSCs, obtained through the reprogramming of somatic cells, offer a good compromise[199]. Patient-specific iPSCs can be combined with organ-on-a-chip technologies to personalize devices, constituting a powerful tool to optimize drug dosages for individual patients[200–202]. Drug responses studied in large populations with different genetic backgrounds are variable[203,204], and iPSCs from patients with genetic mutations could refine drug response studies. Large libraries of iPSCs are available in Europe (for example, by the Wellcome Trust, UK) and in the US (National Institutes of Health and California Institute for Regenerative Medicine)[205]. Disease models have already been generated using cardiomyocytes obtained by differentiating iPSCs from patients with Timothy syndrome[206], long QT[207], LEOPARD[208], Barth[209] syndrome and dilated cardiomyopathy[210]. Gene editing technologies[211,212] could further be used to generate multiple genetic diseases derived from a single healthy stem cell, enabling the production of relevant personalized tissue models.

Pluripotent stem cells can also be expanded into heterogenous cell populations, which can self-organize into organoids. Various epithelial and epithelial–mesenchymal organoids have been developed from human iPSCs, for example, corneal and retinal[213,214], liver[215], pancreas[216,217], gut[218], brain[219], kidney[74] and lung[220] organoids[221]. Organoids are 3D and heterogeneous and thus offer a high level of fidelity in terms of gene and protein expression, tissue morphology and metabolic and physiological functions. However, challenges remain in terms of reproducibility, diffusion, control over perfusion and input–output parameters, applicability of built-in functional readouts and other microenvironmental considerations. The synergistic engineering of organ-on-a-chip and organoid technologies will overcome these challenges and deliver on the promise of precision medicine[75].

Multiplexing and fluid handling. An essential part of organ-on-a-chip technology is fluid handling. The fluid component affects both the precision of control over cellular microenvironments and the strategy for device multiplexing. Different perfusion techniques can be incorporated into organ-on-a-chip devices to enable continuous media recirculation[222]. For example, external pumps (that is, syringe, vacuum or peristaltic pumps)[65,223] can be used, which offer great control of fluid dynamics in microfluidic systems. However, connecting multiple tube setups requires expertise to avoid the formation of air bubbles. The dilution of secreted growth factors in a microfluidic chip using large media reservoirs is also a major concern. In an integrated system, controlling culture parameters, such as supply of nutrients and oxygen, removal of cellular waste and toxins and diffusion of metabolic or angiogenic factors, is crucial to stimulate physiologically relevant crosstalk between cellular components[224]. These factors depend on the correct physiological cell-to-liquid ratio, which can be achieved by maintaining continuous media recirculation in the culture of microtissues using a small amount of media.

To eliminate the need for tubing connections and the use of large media reservoirs, built-in micropumps can be seamlessly integrated into organ-on-a-chip systems to enable media recirculation. These micropumps are often based on pneumatically controlled membrane deflection to drive fluid flow. Multiple micropumps can drive multiple fluid circuits representing different body fluids (for example, blood and urine). Alternatively, they can be programmed to drive fluid recirculation in different combinations of organ models connected in various ways, which is particularly useful for the modelling of physiological hormonal cycles. However, simultaneous perfusion of multiple tissues by built-in micropumps substantially increases the cost of the devices. Alternatively, gravity-driven flow can be employed, which is a simple passive flow technique based on differential fluid pressure in the reservoirs. This setup is inexpensive, can be operated by non-expert users and enables multiplexing in a multiwell plate format, from which fluid can be easily collected by traditional pipetting. The laboratory infrastructure at universities and in pharmaceutical companies is usually equipped with liquid dispensing systems and high-throughput imaging platforms for liquid handling in multiwell plates[77]. Therefore, multiwell plate designs in organ-on-a-chip devices might reduce translational costs and accelerate adaptation for non-expert users[225].

Online sensing of responses. Accurate representation of in vivo organ physiology and drug pharmacokinetics can be achieved in organ-on-a-chip devices through precise control of cellular microenvironments; however, the extraction of quantitative information is equally important. Current on-chip assays heavily rely on fluorescence microscopy and have mainly been used for specialized proof-of-concept studies to investigate angiogenesis[226–228], electrophysiology[225,229] and pharmacological modulation of cell growth[28,118,230]. However, fluorescent labelling is a qualitative method and a terminal assay. Therefore, organ-on-a-chip systems are now being increasingly equipped with sophisticated built-in sensors that provide valuable real-time data on a cellular level, which cannot be easily measured in animal models.

Most on-chip assays depend on either electrochemical or optical-chemical sensing. Metal electrodes or sensitive probe dyes can be directly deposited onto the platforms[231–233], and parameters, such as oxygen concentration[234–236], pH level[237,238] or glucose consumption[239–241], can be monitored to study changes in cellular metabolism. These biosensors are usually based on oxidation–reduction reactions, enzymatic activity, lifetime measurements or ratiometric fluorescence of the probes, and their selectivity and specificity can be improved by specific surface functionalization to enable antibody-based or aptamer-based sensing[242]. This

non-invasive approach enables the detection of small molecules and biomarkers within a complex biological environment with high sensitivity[243–246]. For example, a modular organ-on-a-chip device implementing such sensors can be used to automatically extract quantitative biochemical readouts from recirculating media with high specificity in a multi-organ system[69].

Electrodes can further be used to measure functional changes in tissues in real time. Instead of directly depositing sensory probes or electrodes using multiple lithography steps, a mechanical force sensor can be built by 3D printing of multiple materials in a single continuous step[58]. Specifically, to probe the contraction of laminar cardiac tissues, a conductive ink composed of carbon black nanoparticles can be 3D printed and embedded in a soft thermal plastic polyurethane sheet that supports the growth of cardiomyocytes. The bending of the elastic sheet caused by cardiac cell contraction can lead to a change in the electrical resistance of the embedded conductive circuit[58]. Electrodes can also be used to study the barrier integrity of an endothelium. Gold-based[78,247] or silver/silver-chloride-based[248] electrodes can be incorporated in organ-on-a-chip devices to probe epithelial barrier integrity by measuring the *trans*-epithelial electrical resistance (TEER). This quantitative readout is a useful metric not only for assessing the health of an endothelium but also for studying drug delivery and diffusion in tissues. The development of micro-sensors with high sensitivity presents an opportunity for organ-on-a-chip systems to effectively measure subtle, non-lethal changes in tissue functionality at the cellular level, which is an important advantage over animal testing.

Scalable production. Academic proof-of-concept prototypes cannot be translated into products to solve real-world problems if they do not leave the laboratory. The success of an organ-on-a-chip device depends not only on its scientific validity but also on the ease and scalability of its manufacturing, which can be a considerable hurdle in the commercialization process[36]. Therefore, researchers developing organ-on-a-chip devices should reach out to commercial manufacturers early in the development process, because fabrication protocols at the laboratory scale are often not adaptable to large-scale manufacturing processes. For example, most organ-on-a-chip devices are fabricated by soft lithography, which is a slow and expensive microfabrication technique. Importantly, most devices are manually fabricated involving multiple assembly steps and thus often lack reproducibility or have low production yield. In the manufacturing industry, injection moulding is a common method for the mass production of simple plastic parts. Unfortunately, a device with multilayer fluid circuits and built-in sensors will face additional challenges in terms of post-processing, increasing the manufacturing costs. Therefore, there is a trade-off between device complexity and manufacturability.

3D printing (or additive manufacturing) can be applied to automate and scale up the production of organ-on-a-chip devices in both academic and commercial settings. 3D printing allows for automated and rapid prototyping of devices with complex microarchitectures[249–251]. Using a one-step continuous printing technique, complex multilayer devices composed of multiple materials and sensors can be manufactured in a one-step process. This technique does not require manual handling and has shorter turn-around times and high reproducibility. Thus, 3D printing can provide good manufacturing practice for the fabrication of highly complex devices. Nevertheless, commercialization of organ-on-a-chip devices is likely to be an evolutionary rather than revolutionary process because challenges remain for the automated bioprinting of organ-on-a-chip devices, such as a narrow range of printable and biocompatible materials, issues with resolution and cryopreservation of printed tissues.

Validation of organ-on-a-chip devices. The use of organ-on-a-chip devices in the medical and pharmaceutical industry depends on successful device validation to ensure that the biological functions reproduced on the chip are representative of the native tissues as well as to understand any lack of similarity. An accurate level of understanding is crucial for effective industrial decision making; however, current protocols to validate in vitro models are limited[203]. A direct comparison against current industry standards as well as between different technologies might be necessary for the translation of in vitro tissue technologies. To better meet the needs and standards of the pharmaceutical industry, many organ-on-a-chip systems are being developed in collaboration between academic laboratories and industry to improve the biological relevance of the devices as early as possible[252]. For example, Emulate is collaborating with Johnson & Johnson to use organ-on-a-chip devices in two applications: Lung-on-Chip and Thrombosis-on-Chip to evaluate pulmonary thrombosis and Liver-on-Chip to better predict liver toxicity. TissUse GmbH is working together with the cosmetic company Beiersdorf AG, and Mimetas is developing high-throughput intestinal models in collaboration with Roche. Regulatory agencies (for example, the US Food and Drug Administration, FDA) have also begun to collaborate with the pharmaceutical industry to establish industry standards and suitable physiological hallmarks for the validation of organ-on-a-chip devices[253,254]. Such initiatives include the Comprehensive In Vitro Proarrythmia Assay Initiative (CiPA Initiative) and the International Consortium for Innovation and Quality in Pharmaceutical Development (IQ Consortium). Other organizations, such as the National Institute of Diabetes and Digestive and Kidney Diseases (NIDDK) (US National Institutes of Health (NIH), National Institute of Biomedical Imaging and Bioengineering), the American Institute for Medical and Biological Engineering (American Institute for Medical and Biological Engineering (AIMBE)) and the National Institute of Biomedical Imaging and Bioengineering (NIBIB) (NIH, National Institute of Biomedical Imaging and Bioengineering), have also developed their own initiatives in this space.

We have further proposed a drug discovery pipeline for cardiac functional assessments of kinase inhibitors in a lab setting, involving high-throughput screening of cytokines on cardiomyocyte monolayers, target

identification by machine learning and target validation using a 3D Biowire platform[255]. Machine learning can be applied to unbiasedly select compounds from the high-throughput monolayer screen. Selected compounds can be further investigated with 3D tissue models. High-throughput monolayer screens provide a quick and cost-effective readout of a few simple parameters for many compounds, and 3D tissues enable the assessment of in-depth functional parameters owing to their maturity and 3D complexity. Therefore, key steps for organ-on-a-chip technology to be accepted for preclinical testing might be reproducing results obtained with established methods and refining results in conjunction with clinical data, which might ultimately lead to a new preclinical paradigm for drug testing. Organ-on-a-chip technology is unlikely to replace animal testing in the near future; however, organ-on-a-chip devices can generate independent data sets that can be used to augment various stages of the drug discovery pipeline to obtain precise information on the effect of a drug before human clinical trials. If organ-on-a-chip systems prove to be able to consistently and accurately predict the effects of drugs, a paradigm shift of preclinical drug testing towards in vitro 3D human tissue models is possible, which is not only more human but also more humane than animal models.

Published online: 01 August 2018

1. Shehab, N. et al. US emergency department visits for outpatient adverse drug events, 2013–2014. *JAMA* **316**, 2115–2125 (2016).
2. Shahrbaf, F. G. & Assadi, F. Drug-induced renal disorders. *J. Renal Injury Prevention* **4**, 57 (2015).
3. Kim, S. Y. & Moon, A. Drug-induced nephrotoxicity and its biomarkers. *Biomolecules Ther.* **20**, 268 (2012).
4. Adams, C. P. & Brantner, V. V. Spending on new drug development1. *Health Econom.* **19**, 130–141 (2010).
5. Kinch, M. S. & Merkel, J. An analysis of FDA-approved drugs for inflammation and autoimmune diseases. *Drug Discov. Today* **20**, 920–923 (2015).
6. DiMasi, J. A., Grabowski, H. G. & Hansen, R. W. Innovation in the pharmaceutical industry: new estimates of R&D costs. *J. Health Econom.* **47**, 20–33 (2016).
7. Paul, S. M. et al. How to improve R&D productivity: the pharmaceutical industry's grand challenge. *Nat. Rev. Drug Discov.* **9**, 203–214 (2010).
8. Ben-David, U. et al. Patient-derived xenografts undergo mouse-specific tumor evolution. *Nat. Genet.* **49**, 1567–1575 (2017).
9. Rohr, S., Schölly, D. M. & Kleber, A. G. Patterned growth of neonatal rat heart cells in culture. Morphological and electrophysiological characterization. *Circul. Res.* **68**, 114–130 (1991).
10. Fast, V. G., Rohr, S., Gillis, A. M. & Kléber, A. G. Activation of cardiac tissue by extracellular electrical shocks: formation of 'secondary sources' at intercellular clefts in monolayers of cultured myocytes. *Circul. Res.* **82**, 375–385 (1998).
11. Kucera, J. P., Kléber, A. G. & Rohr, S. Slow conduction in cardiac tissue, II: effects of branching tissue geometry. *Circul. Res.* **83**, 795–805 (1998).
12. Rohr, S., Kucera, J. P. & Kléber, A. G. Slow conduction in cardiac tissue, I: effects of a reduction of excitability versus a reduction of electrical coupling on microconduction. *Circul. Res.* **83**, 781–794 (1998).
13. Rohr, S., Kucera, J. P., Fast, V. G. & Kléber, A. G. Paradoxical improvement of impulse conduction in cardiac tissue by partial cellular uncoupling. *Science* **275**, 841–844 (1997).
14. Duffy, D. C., McDonald, J. C., Schueller, O. J. & Whitesides, G. M. Rapid prototyping of microfluidic systems in poly(dimethylsiloxane). *Anal. Chem.* **70**, 4974–4984 (1998).
15. Xia, Y. & Whitesides, G. M. Soft lithography. *Annu. Rev. Mater. Sci.* **28**, 153–184 (1998).
16. Whitesides, G. M. The origins and the future of microfluidics. *Nature* **442**, 368 (2006).
17. Sin, A. et al. The design and fabrication of three-chamber microscale cell culture analog devices with integrated dissolved oxygen sensors. *Biotechnol. Progress* **20**, 338–345 (2004).
18. Viravaidya, K., Sin, A. & Shuler, M. L. Development of a microscale cell culture analog to probe naphthalene toxicity. *Biotechnol. Progress* **20**, 316–323 (2004).
19. Song, J. W. et al. Computer-controlled microcirculatory support system for endothelial cell culture and shearing. *Anal. Chem.* **77**, 3993–3999 (2005).
20. Lam, M. T., Huang, Y.-C., Birla, R. K. & Takayama, S. Microfeature guided skeletal muscle tissue engineering for highly organized 3-dimensional free-standing constructs. *Biomaterials* **30**, 1150–1155 (2009).
21. Jang, K., Sato, K., Igawa, K., Chung, U.-i. & Kitamori, T. Development of an osteoblast-based 3D continuous-perfusion microfluidic system for drug screening. *Anal. Bioanal. Chem.* **390**, 825–832 (2008).
22. Huh, D. et al. Acoustically detectable cellular-level lung injury induced by fluid mechanical stresses in microfluidic airway systems. *Proc. Natl Acad. Sci. USA* **104**, 18886–18891 (2007).
23. Carraro, A. et al. In vitro analysis of a hepatic device with intrinsic microvascular-based channels. *Biomed. Microdevices* **10**, 795–805 (2008).
24. Lee, P. J., Hung, P. J. & Lee, L. P. An artificial liver sinusoid with a microfluidic endothelial-like barrier for primary hepatocyte culture. *Biotechnol. Bioeng.* **97**, 1340–1346 (2007).
25. Harris, S. G. & Shuler, M. L. Growth of endothelial cells on microfabricated silicon nitride membranes for an in vitro model of the blood-brain barrier. *Biotechnol. Bioprocess Eng.* **8**, 246–251 (2003).
26. Mahler, G. J., Esch, M. B., Glahn, R. P. & Shuler, M. L. Characterization of a gastrointestinal tract microscale cell culture analog used to predict drug toxicity. *Biotechnol. Bioeng.* **104**, 193–205 (2009).
27. Kimura, H., Yamamoto, T., Sakai, H., Sakai, Y. & Fujii, T. An integrated microfluidic system for long-term perfusion culture and on-line monitoring of intestinal tissue models. *Lab. Chip* **8**, 741–746 (2008).
28. Jang, K.-J. & Suh, K.-Y. A multi-layer microfluidic device for efficient culture and analysis of renal tubular cells. *Lab. Chip* **10**, 36–42 (2010).
29. Huh, D. et al. Reconstituting organ-level lung functions on a chip. *Science* **328**, 1662–1668 (2010).
This is a landmark study on recapitulating organ-level lung function in vitro with a microfluidic chip.
30. Ingber, D. E. Reverse engineering human pathophysiology with organs-on-chips. *Cell* **164**, 1105–1109 (2016).
31. Langer, R. & Vacanti, J. P. Tissue engineering. *Science* **260**, 920–926 (1993).
32. El-Ali, J., Sorger, P. K. & Jensen, K. F. Cells on chips. *Nature* **442**, 403–411 (2006).
33. Takahashi, K. & Yamanaka, S. Induction of pluripotent stem cells from mouse embryonic and adult fibroblast cultures by defined factors. *Cell* **126**, 663–676 (2006).
34. Park, I.-H. et al. Reprogramming of human somatic cells to pluripotency with defined factors. *Nature* **451**, 141–146 (2008).
35. Reardon, S. Organs-on-chips' go mainstream: drug companies put in vitro systems through their paces. *Nature* **523**, 266–267 (2015).
36. Zhang, B. & Radisic, M. Organ-on-a-Chip devices advance to market. *Lab. Chip* **17**, 2395–2420 (2017).
This is a comprehensive review on organ-on-a-chip start-ups in the market space.
37. Zheng, Y., Chen, J. & López, J. A. Flow-driven assembly of VWF fibres and webs in in vitro microvessels. *Nat. Commun.* **6**, 7858 (2015).
38. Zheng, Y. et al. In vitro microvessels for the study of angiogenesis and thrombosis. *Proc. Natl Acad. Sci. USA* **109**, 9342–9347 (2012).
39. Jang, K.-J. et al. Human kidney proximal tubule-on-a-chip for drug transport and nephrotoxicity assessment. *Integr. Biol.* **5**, 1119–1129 (2013).
40. Kim, H. J., Huh, D., Hamilton, G. & Ingber, D. E. Human gut-on-a-chip inhabited by microbial flora that experiences intestinal peristalsis-like motions and flow. *Lab. Chip* **12**, 2165–2174 (2012).
41. Benam, K. H. et al. Small airway-on-a-chip enables analysis of human lung inflammation and drug responses in vitro. *Nat. Methods* **13**, 151–157 (2016).
42. Musah, S. et al. Mature induced-pluripotent-stem-cell-derived human podocytes reconstitute kidney glomerular-capillary-wall function on a chip. *Nat. Biomed. Eng.* **1**, 0069 (2017).
43. Adriani, G., Ma, D., Pavesi, A., Kamm, R. D. & Goh, E. L. A. 3D neurovascular microfluidic model consisting of neurons, astrocytes and cerebral endothelial cells as a blood–brain barrier. *Lab. Chip* (2017).
44. Jeon, J. S. et al. Human 3D vascularized organotypic microfluidic assays to study breast cancer cell extravasation. *Proc. Natl Acad. Sci. USA* **112**, 214–219 (2015).
45. Trietsch, S. J. et al. Membrane-free culture and real-time barrier integrity assessment of perfused intestinal epithelium tubes. *Nat. Commun.* **8**, 262 (2017).
46. Adler, M. et al. A quantitative approach to screen for nephrotoxic compounds in vitro. *J. Am. Soc. Nephrol.* **27**, 1015–1028 (2016).
47. Homan, K. A. et al. Bioprinting of 3D convoluted renal proximal tubules on perfusable chips. *Sci. Rep.* **6**, 34845 (2016).
48. Weber, E. J. et al. Development of a microphysiological model of human kidney proximal tubule function. *Kidney Int.* **90**, 627–637 (2016).
49. Shlomai, A. et al. Modeling host interactions with hepatitis B virus using primary and induced pluripotent stem cell-derived hepatocellular systems. *Proc. Natl Acad. Sci. USA* **111**, 12193–12198 (2014).
50. Khetani, S. R. & Bhatia, S. N. Microscale culture of human liver cells for drug development. *Nat. Biotechnol.* **26**, 120–126 (2008).
51. Frey, O., Misun, P. M., Fluri, D. A., Hengstler, J. G. & Hierlemann, A. Reconfigurable microfluidic hanging drop network for multi-tissue interaction and analysis. *Nat. Commun.* **5**, 4250 (2014).
52. Yazdi, S. R. et al. Adding the 'heart'to hanging drop networks for microphysiological multi-tissue experiments. *Lab. Chip* **15**, 4138–4147 (2015).
53. Nguyen, D. G. et al. Bioprinted 3D primary liver tissues allow assessment of organ-level response to clinical drug induced toxicity in vitro. *PLoS One* **11**, e0158674 (2016).
54. Nunes, S. S. et al. Biowire: a platform for maturation of human pluripotent stem cell-derived cardiomyocytes. *Nat. Methods* **10**, 781–787 (2013).
This is a study on the maturation of engineered human cardiac tissues with electrical stimulation.
55. Mathur, A. et al. Human iPSC-based cardiac microphysiological system for drug screening applications. *Sci. Rep.* **5**, 8883 (2015).
56. Legant, W. R. et al. Microfabricated tissue gauges to measure and manipulate forces from 3D microtissues. *Proc. Natl Acad. Sci. USA* **106**, 10097–10102 (2009).
57. Jackman, C. P., Carlson, A. L. & Bursac, N. Dynamic culture yields engineered myocardium with near-adult functional output. *Biomaterials* **111**, 66–79 (2016).
58. Lind, J. U. et al. Instrumented cardiac microphysiological devices via multimaterial three-dimensional printing. *Nat. Mater.* **16**, 303–308 (2016).
This study presents an entirely 3D-printed platform for the culture and analysis of engineered cardiac tissues.
59. Sidorov, V. Y. et al. I-Wire Heart-on-a-Chip I: three-dimensional cardiac tissue constructs for physiology and pharmacology. *Acta Biomaterialia* **48**, 68–78 (2017).
60. Zimmermann, W.-H. et al. Engineered heart tissue grafts improve systolic and diastolic function in infarcted rat hearts. *Nat. Med.* **12**, 452–458 (2006).
61. Wittmann, K. & Fischbach, C. Contextual control of adipose-derived stem cell function: implications for

engineered tumor models. *ACS Biomater. Sci. Eng.* **3**, 1483–1493 (2016).

62. Miller, P. G. & Shuler, M. L. Design and demonstration of a pumpless 14 compartment microphysiological system. *Biotechnol. Bioeng.* **113**, 2213–2227 (2016).
This study presents a body-on-a-chip platform integrated with 14 tissue compartments.
63. Oleaga, C. et al. Multi-Organ toxicity demonstration in a functional human in vitro system composed of four organs. *Sci. Rep.* **6**, 20030 (2016).
64. Xiao, S. et al. A microfluidic culture model of the human reproductive tract and 28-day menstrual cycle. *Nat. Commun.* **8**, 14584 (2017).
65. Coppeta, J. et al. A portable and reconfigurable multi-organ platform for drug development with onboard microfluidic flow control. *Lab. Chip* **17**, 134–144 (2017).
66. Vernetti, L. et al. Functional coupling of human microphysiology systems: intestine, liver, kidney proximal tubule, blood-brain barrier and skeletal muscle. *Sci. Rep.* **7**, 42296 (2017).
This is a study on multi-organ interaction with multiple decentralized organ-on-a-chip systems located at different sites.
67. Maschmeyer, I. et al. A four-organ-chip for interconnected long-term co-culture of human intestine, liver, skin and kidney equivalents. *Lab. Chip* **15**, 2688–2699 (2015).
68. Loskill, P., Marcus, S. G., Mathur, A., Reese, W. M. & Healy, K. E. μOrgano: A Lego®-like plug & play system for modular multi-organ-chips. *PLoS One* **10**, e0139587 (2015).
69. Zhang, Y. S. et al. Multisensor-integrated organs-on-chips platform for automated and continual in situ monitoring of organoid behaviors. *Proc. Natl Acad. Sci. USA* **114**, E2293–E2302 (2017).
70. Zhang, B. et al. Biodegradable scaffold with built-in vasculature for organ-on-a-chip engineering and direct surgical anastomosis. *Nat. Mater.* **15**, 669–678 (2016).
This study presents a biodegradable scaffold with a built-in blood vessel network that supports both organ-on-a-chip engineering and in vivo implantation.
71. Kolesky, D. B., Homan, K. A., Skylar-Scott, M. A. & Lewis, J. A. Three-dimensional bioprinting of thick vascularized tissues. *Proc. Natl Acad. Sci. USA* **113**, 3179–3184 (2016).
72. Miller, J. S. et al. Rapid casting of patterned vascular networks for perfusable engineered three-dimensional tissues. *Nat. Mater.* **11**, 768–774 (2012).
This study discusses the rapid fabrication of microfluidic networks in hydrogel matrices by 3D printing of sacrificial materials.
73. Kang, H.-W. et al. A 3D bioprinting system to produce human-scale tissue constructs with structural integrity. *Nat. Biotechnol.* **34**, 312–319 (2016).
74. Takasato, M. et al. Kidney organoids from human iPS cells contain multiple lineages and model human nephrogenesis. *Nature* **526**, 564–568 (2015).
75. Takebe, T., Zhang, B. & Radisic, M. Synergistic engineering: organoids meet organs-on-a-chip. *Cell Stem Cell* **21**, 297–300 (2017).
This is a review that promotes the integration of organoids and organs-on-a-chip as a future step in the field.
76. Berthier, E., Young, E. W. & Beebe, D. Engineers are from PDMS-land, biologists are from polystyrenia. *Lab. Chip* **12**, 1224–1237 (2012).
77. Junaid, A., Mashaghi, A., Hankemeier, T. & Vulto, P. An end-user perspective on Organ-on-a-Chip: assays and usability aspects. *Curr. Opin. Biomed. Engineer.* **1**, 15–22 (2017).
78. Maoz, B. M. et al. Organs-on-Chips with combined multi-electrode array and transepithelial electrical resistance measurement capabilities. *Lab. Chip* **17**, 2294–2302 (2017).
79. Ingber, D. E. Cellular mechanotransduction: putting all the pieces together again. *FASEB J.* **20**, 811–827 (2006).
80. Huh, D. et al. A human disease model of drug toxicity–induced pulmonary edema in a lung-on-a-chip microdevice. *Sci. Transl Med.* **4**, 159ra147 (2012).
81. Huh, D. et al. Microfabrication of human organs-on-chips. *Nat. Protoc.* **8**, 2135–2157 (2013).
82. Benam, K. H. et al. Matched-comparative modeling of normal and diseased human airway responses using a microengineered breathing lung chip. *Cell Systems* **3**, 416–418 (2016).
83. Kim, H. J., Li, H., Collins, J. J. & Ingber, D. E. Contributions of microbiome and mechanical deformation to intestinal bacterial overgrowth and inflammation in a human gut-on-a-chip. *Proc. Natl Acad. Sci. USA* **113**, E7–E15 (2016).
84. Villenave, R. et al. Human Gut-on-a-Chip supports polarized infection of coxsackie B1 virus in vitro. *PLoS One* **12**, e0169412 (2017).
85. Kim, S. et al. Pharmacokinetic profile that reduces nephrotoxicity of gentamicin in a perfused kidney-on-a-chip. *Biofabrication* **8**, 015021 (2016).
86. Tavana, H., Zamankhan, P., Christensen, P. J., Grotberg, J. B. & Takayama, S. Epithelium damage and protection during reopening of occluded airways in a physiologic microfluidic pulmonary airway model. *Biomed. Microdevices* **13**, 731–742 (2011).
87. Tavana, H. et al. Dynamics of liquid plugs of buffer and surfactant solutions in a micro-engineered pulmonary airway model. *Langmuir* **26**, 3744–3752 (2009).
88. Blundell, C. et al. A microphysiological model of the human placental barrier. *Lab. Chip* **16**, 3065–3073 (2016).
89. Choi, Y. et al. A microengineered pathophysiological model of early-stage breast cancer. *Lab. Chip* **15**, 3350–3357 (2015).
90. Heles, T. Emulate expands series B to $45m. *Global University Venturing* http://www.globaluniversityventuring.com/article.php/5521/emulate-expands-series-b-to-45m (2016).
91. Bouchie, A. & DeFrancesco, L. *Nature Biotechnology*'s academic spinouts of 2014. *Nat. Biotechnol.* **33**, 247–255 (2015).
92. Timmerman, L. Organ-on-a-Chip startup, Emulate, grabs $45m to shake up drug discovery. *Forbes* https://www.forbes.com/sites/luketimmerman/2016/10/20/organ-on-a-chip-startup-emulate-grabs-45m-to-improve-drug-discovery/#3b20b0825fcb (2016).
93. Choi, N. W. et al. Microfluidic scaffolds for tissue engineering. *Nat. Mater.* **6**, 908–915 (2007).
94. Leach, J. B. & Schmidt, C. E. Characterization of protein release from photocrosslinkable hyaluronic acid-polyethylene glycol hydrogel tissue engineering scaffolds. *Biomaterials* **26**, 125–135 (2005).
95. Ligresti, G. et al. A novel three-dimensional human peritubular microvascular system. *J. Am. Soc. Nephrol.* **27**, 2370–2381 (2015).
96. Tourovskaia, A., Fauver, M., Kramer, G., Simonson, S. & Neumann, T. Tissue-engineered microenvironment systems for modeling human vasculature. *Exp. Biol. Med.* **239**, 1264–1271 (2014).
97. Stucki, A. O. et al. A lung-on-a-chip array with an integrated bio-inspired respiration mechanism. *Lab. Chip* **15**, 1302–1310 (2015).
98. Gu, Z. Integrating intelligent materials into organ on a chip system (abstract W4B.1). *Proceedings International Conference on Photonics and Imaging in Biology and Medicine* (2017).
99. Moreno, E. L. et al. Differentiation of neuroepithelial stem cells into functional dopaminergic neurons in 3D microfluidic cell culture. *Lab. Chip* **15**, 2419–2428 (2015).
100. Trietsch, S. J., Israëls, G. D., Joore, J., Hankemeier, T. & Vulto, P. Microfluidic titer plate for stratified 3D cell culture. *Lab. Chip* **13**, 3548–3554 (2013).
101. Duinen, V. v. et al. 96 perfusable blood vessels to study vascular permeability in vitro. *Sci. Rep.* **7**, 18071 (2017).
102. Jeon, N. L. In vitro formation and characterization of a perfusable three-dimensional tubular capillary network in microfluidic devices. *Lab. Chip* **12**, 2815–2822 (2012).
103. Kim, S., Lee, H., Chung, M. & Jeon, N. L. Engineering of functional, perfusable 3D microvascular networks on a chip. *Lab. Chip* **13**, 1489–1500 (2013).
104. Shin, Y. et al. Microfluidic assay for simultaneous culture of multiple cell types on surfaces or within hydrogels. *Nat. Protoc.* **7**, 1247–1259 (2012).
105. Chung, S. et al. Cell migration into scaffolds under co-culture conditions in a microfluidic platform. *Lab. Chip* **9**, 269–275 (2009).
106. Wang, X. et al. An on-chip microfluidic pressure regulator that facilitates reproducible loading of cells and hydrogels into microphysiological system platforms. *Lab. Chip* **16**, 868–876 (2016).
107. Wang, X. et al. Engineering anastomosis between living capillary networks and endothelial cell-lined microfluidic channels. *Lab. Chip* **16**, 282–290 (2016).
108. Moya, M. L., Hsu, Y.-H., Lee, A. P., Hughes, C. C. & George, S. C. In vitro perfused human capillary networks. *Tissue Eng. Part C Methods* **19**, 730–737 (2013).
109. Hsu, Y.-H., Moya, M. L., Hughes, C. C., George, S. C. & Lee, A. P. A microfluidic platform for generating large-scale nearly identical human microphysiological vascularized tissue arrays. *Lab. Chip* **13**, 2990–2998 (2013).
110. Wiedeman, M. P. Dimensions of blood vessels from distributing artery to collecting vein. *Circul. Res.* **12**, 375–378 (1963).
111. Polacheck, W. J., German, A. E., Mammoto, A., Ingber, D. E. & Kamm, R. D. Mechanotransduction of fluid stresses governs 3D cell migration. *Proc. Natl Acad. Sci. USA* **111**, 2447–2452 (2014).
112. Aref, A. R. et al. Screening therapeutic EMT blocking agents in a three-dimensional microenvironment. *Integr. Biol.* **5**, 381–389 (2013).
113. Vickerman, V. & Kamm, R. D. Mechanism of a flow-gated angiogenesis switch: early signaling events at cell–matrix and cell–cell junctions. *Integr. Biol.* **4**, 863–874 (2012).
114. Chung, M., Kim, S., Ahn, J., Lee, S. & Jeon, N. L. Interstitial flow regulates angiogenic response and phenotype of endothelial cells in a 3D culture model. *Lab. Chip* **16**, 4189–4199 (2016).
115. Phan, D. T. et al. A vascularized and perfused organ-on-a-chip platform for large-scale drug screening applications. *Lab. Chip* **17**, 511–520 (2017).
116. LiâJeon, N. Microfluidic vascularized bone tissue model with hydroxyapatite-incorporated extracellular matrix. *Lab. Chip* **15**, 3984–3988 (2015).
117. Zervantonakis, I. K. et al. Three-dimensional microfluidic model for tumor cell intravasation and endothelial barrier function. *Proc. Natl Acad. Sci. USA* **109**, 13515–13520 (2012).
118. Sobrino, A. et al. 3D microtumors in vitro supported by perfused vascular networks. *Sci. Rep.* **6**, 31589 (2016).
119. Oh, S. et al. "Open-top" microfluidic device for in vitro three-dimensional capillary beds. *Lab. Chip* **17**, 3405–3414 (2017).
120. Nashimoto, Y. et al. Integrating perfusable vascular networks with a three-dimensional tissue in a microfluidic device. *Integr. Biol.* **9**, 506–518 (2017).
121. Kim, S., Chung, M. & Jeon, N. L. Three-dimensional biomimetic model to reconstitute sprouting lymphangiogenesis in vitro. *Biomaterials* **78**, 115–128 (2016).
122. Wadman, M. Merck settles Vioxx lawsuits for $4.85 billion. *Nature* **450**, 324 (2007).
123. Kattman, S. J. et al. Stage-specific optimization of activin/nodal and BMP signaling promotes cardiac differentiation of mouse and human pluripotent stem cell lines. *Cell Stem Cell* **8**, 228–240 (2011).
124. Radisic, M. et al. Functional assembly of engineered myocardium by electrical stimulation of cardiac myocytes cultured on scaffolds. *Proc. Natl Acad. Sci. USA* **101**, 18129–18134 (2004).
125. Tandon, N. et al. Electrical stimulation systems for cardiac tissue engineering. *Nat. Protoc.* **4**, 155–173 (2009).
126. Stoehr, A. et al. Spontaneous formation of extensive vessel-like structures in murine engineered heart tissue. *Tissue Eng. Part A* **22**, 326–335 (2016).
127. Mannhardt, I. et al. Human engineered heart tissue: analysis of contractile force. *Stem Cell Rep.* **7**, 29–42 (2016).
128. Eder, A., Vollert, I., Hansen, A. & Eschenhagen, T. Human engineered heart tissue as a model system for drug testing. *Adv. Drug Deliv. Rev.* **96**, 214–224 (2016).
129. Zimmermann, W.-H. et al. Tissue engineering of a differentiated cardiac muscle construct. *Circul. Res.* **90**, 223–230 (2002).
130. Bian, W., Badie, N., Himel IV, H. D. & Bursac, N. Robust T-tubulation and maturation of cardiomyocytes using tissue-engineered epicardial mimetics. *Biomaterials* **35**, 3819–3828 (2014).
131. Vunjak-Novakovic, G., Bhatia, S., Chen, C. & Hirschi, K. HeLiVa platform: integrated heart-liver-vascular systems for drug testing in human health and disease. *Stem Cell Res. Ther.* **4**, S8 (2013).
132. Wilson, K., Das, M., Wahl, K. J., Colton, R. J. & Hickman, J. Measurement of contractile stress generated by cultured rat muscle on silicon cantilevers for toxin detection and muscle performance enhancement. *PLoS One* **5**, e11042 (2010).
133. Schroer, A. K., Shotwell, M. S., Sidorov, V. Y., Wikswo, J. P. & Merryman, W. D. I-Wire Heart-on-a-Chip II: biomechanical analysis of contractile, three-dimensional cardiomyocyte tissue constructs. *Acta Biomaterialia* **48**, 79–87 (2017).

134. Watkins, P. B. et al. The clinical liver safety assessment best practices workshop: rationale, goals, accomplishments and the future. *Drug Safety* **37**, 1–7 (2014).
135. Lucena, M. I. et al. Trovafloxacin-induced acute hepatitis. *Clin. Infect. Dis.* **30**, 400–401 (2000).
136. Bhatia, S., Balis, U., Yarmush, M. & Toner, M. Effect of cell–cell interactions in preservation of cellular phenotype: cocultivation of hepatocytes and nonparenchymal cells. *FASEB J.* **13**, 1883–1900 (1999).
137. Hui, E. E. & Bhatia, S. N. Micromechanical control of cell–cell interactions. *Proc. Natl Acad. Sci. USA* **104**, 5722–5726 (2007).
138. Stevens, K. et al. InVERT molding for scalable control of tissue microarchitecture. *Nat. Commun.* **4**, 1847 (2013).
139. Ware, B. R., Berger, D. R. & Khetani, S. R. Prediction of drug-induced liver injury in micropatterned co-cultures containing iPSC-derived human hepatocytes. *Toxicol. Sci.* **145**, 252–262 (2015).
140. Ploss, A. et al. Persistent hepatitis C virus infection in microscale primary human hepatocyte cultures. *Proc. Natl Acad. Sci. USA* **107**, 3141–3145 (2010).
141. Khetani, S. R. et al. Use of micropatterned cocultures to detect compounds that cause drug-induced liver injury in humans. *Toxicol. Sci.* **132**, 107–117 (2013).
142. Xu, J. J. et al. Cellular imaging predictions of clinical drug-induced liver injury. *Toxicol. Sci.* **105**, 97–105 (2008).
143. Nguyen, T. V. et al. Establishment of a hepatocyte-kupffer cell coculture model for assessment of proinflammatory cytokine effects on metabolizing enzymes and drug transporters. *Drug Metab. Dispos.* **43**, 774–785 (2015).
144. Stevens, K. R. et al. In situ expansion of engineered human liver tissue in a mouse model of chronic liver disease. *Sci. Transl Med.* **9**, eaah5505 (2017).
145. Jakab, K., Neagu, A., Mironov, V., Markwald, R. R. & Forgacs, G. Engineering biological structures of prescribed shape using self-assembling multicellular systems. *Proc. Natl Acad. Sci. USA* **101**, 2864–2869 (2004).
146. Norotte, C., Marga, F. S., Niklason, L. E. & Forgacs, G. Scaffold-free vascular tissue engineering using bioprinting. *Biomaterials* **30**, 5910–5917 (2009).
147. Jakab, K. et al. Tissue engineering by self-assembly and bio-printing of living cells. *Biofabrication* **2**, 022001 (2010).
148. Norona, L. M., Nguyen, D. G., Gerber, D. A., Presnell, S. C. & LeCluyse, E. L. Modeling compound-induced fibrogenesis in vitro using three-dimensional bioprinted human liver tissues. *Toxicol. Sci.* **154**, 354–367 (2016).
149. Rodenhizer, D. et al. A three-dimensional engineered tumour for spatial snapshot analysis of cell metabolism and phenotype in hypoxic gradients. *Nat. Mater.* **15**, 227–234 (2016).
150. Kelm, J. M., Timmins, N. E., Brown, C. J., Fussenegger, M. & Nielsen, L. K. Method for generation of homogeneous multicellular tumor spheroids applicable to a wide variety of cell types. *Biotechnol. Bioeng.* **83**, 173–180 (2003).
151. Kelm, J. M. & Fussenegger, M. Microscale tissue engineering using gravity-enforced cell assembly. *Trends Biotechnol.* **22**, 195–202 (2004).
152. Kim, J.-Y. et al. 3D spherical microtissues and microfluidic technology for multi-tissue experiments and analysis. *J. Biotechnol.* **205**, 24–35 (2015).
153. Falkenberg, N. et al. Three-dimensional microtissues essentially contribute to preclinical validations of therapeutic targets in breast cancer. *Cancer Med.* **5**, 703–710 (2016).
154. Horman, S. R. et al. High-content analysis of three-dimensional tumor spheroids: Investigating signaling pathways using small hairpin RNA. *Nat. Methods* **10**, 1036 (2013).
155. Wagner, I. et al. A dynamic multi-organ-chip for long-term cultivation and substance testing proven by 3D human liver and skin tissue co-culture. *Lab. Chip* **13**, 3538–3547 (2013).
156. Chung, K. et al. A microfluidic array for large-scale ordering and orientation of embryos. *Nat. Methods* **8**, 171–176 (2011).
157. Levario, T. J., Zhan, M., Lim, B., Shvartsman, S. Y. & Lu, H. Microfluidic trap array for massively parallel imaging of *Drosophila* embryos. *Nat. Protoc.* **8**, 721 (2013).
158. Jackson, E. & Lu, H. Three-dimensional models for studying development and disease: moving on from organisms to organs-on-a-chip and organoids. *Integr. Biol.* **8**, 672–683 (2016).
159. Jackson-Holmes, E., McDevitt, T. C. & Lu, H. A microfluidic trap array for longitudinal monitoring and multi-modal phenotypic analysis of individual stem cell aggregates. *Lab. Chip* **17**, 3634–3642 (2017).
160. Atienzar, F. A. et al. Predictivity of dog co-culture model, primary human hepatocytes and HepG2 cells for the detection of hepatotoxic drugs in humans. *Toxicol. Appl. Pharmacol.* **275**, 44–61 (2014).
161. Novik, E., Maguire, T. J., Chao, P., Cheng, K. & Yarmush, M. L. A microfluidic hepatic coculture platform for cell-based drug metabolism studies. *Biochem. Pharmacol.* **79**, 1036–1044 (2010).
162. Tatosian, D. A. & Shuler, M. L. A novel system for evaluation of drug mixtures for potential efficacy in treating multidrug resistant cancers. *Biotechnol. Bioeng.* **103**, 187–198 (2009).
163. Kidambi, S. et al. Oxygen-mediated enhancement of primary hepatocyte metabolism, functional polarization, gene expression, and drug clearance. *Proc. Natl Acad. Sci. USA* **106**, 15714–15719 (2009).
164. Chao, P., Maguire, T., Novik, E., Cheng, K.-C. & Yarmush, M. Evaluation of a microfluidic based cell culture platform with primary human hepatocytes for the prediction of hepatic clearance in human. *Biochem. Pharmacol.* **78**, 625–632 (2009).
165. Wikswo, J. P. et al. Scaling and systems biology for integrating multiple organs-on-a-chip. *Lab. Chip* **13**, 3496–3511 (2013).
166. Moraes, C. et al. On being the right size: scaling effects in designing a human-on-a-chip. *Integr. Biol.* **5**, 1149–1161 (2013).
167. Esch, M. B., Ueno, H., Applegate, D. R. & Shuler, M. L. Modular, pumpless body-on-a-chip platform for the co-culture of GI tract epithelium and 3D primary liver tissue. *Lab. Chip* **16**, 2719–2729 (2016).
168. Esch, M. B., Mahler, G. J., Stokol, T. & Shuler, M. L. Body-on-a-chip simulation with gastrointestinal tract and liver tissues suggests that ingested nanoparticles have the potential to cause liver injury. *Lab. Chip* **14**, 3081–3092 (2014).
169. Sung, J. H. & Shuler, M. L. A micro cell culture analog (μCCA) with 3D hydrogel culture of multiple cell lines to assess metabolism-dependent cytotoxicity of anti-cancer drugs. *Lab. Chip* **9**, 1385–1394 (2009).
170. Materne, E.-M. et al. The multi-organ chip-a microfluidic platform for long-term multi-tissue coculture. *J. Vis. Exp.* **98**, e52526 (2015).
171. Bauer, S. et al. Functional coupling of human pancreatic islets and liver spheroids on-a-chip: Towards a novel human ex vivo type 2 diabetes model. *Sci. Rep.* **7**, 14620 (2017).
172. Loskill, P. et al. WAT-on-a-chip: a physiologically relevant microfluidic system incorporating white adipose tissue. *Lab. Chip* **17**, 1645–1654 (2017).
173. Yu, J. et al. Quantitative systems pharmacology approaches applied to microphysiological systems (MPS): data interpretation and multi-MPS integration. *CPT Pharmacometrics Syst. Pharmacol.* **4**, 585–594 (2015).
174. Wikswo, J. P. & Porter, A. P. Biology coming full circle: joining the whole and the parts. *Exp. Biol. Med.* **240**, 3–7 (2015).
175. Lai, B. F. L. et al. InVADE: integrated vasculature for assessing dynamic events. *Adv. Funct. Mater.* https://doi.org/10.1002/adfm.201703524 (2017). **This study presents an organ-on-a-chip platform in the format of a multiwell plate that can model inter-organ cancer metastasis**.
176. Yarmush, M. L., Freedman, R., Del Bufalo, A., Teissier, S. & Meunier, J.-R. Immune system modeling devices and methods. Patent application number US9535056B2 (2017).
177. Vargesson, N. Thalidomide-induced teratogenesis: history and mechanisms. *Birth Defects Res. C Embryo Today* **105**, 140–156 (2015).
178. Therapontos, C., Erskine, L., Gardner, E. R., Figg, W. D. & Vargesson, N. Thalidomide induces limb defects by preventing angiogenic outgrowth during early limb formation. *Proc. Natl Acad. Sci. USA* **106**, 8573–8578 (2009).
179. Nawroth, J., Rogal, J., Weiss, M., Brucker, S. Y. & Loskill, P. Organ-on-a-Chip systems for women's health applications. *Adv. Healthc. Mater.* https://doi.org/10.1002/adhm.201700550 (2017).
180. Jo, B.-H., Van Lerberghe, L. M., Motsegood, K. M. & Beebe, D. J. Three-dimensional micro-channel fabrication in polydimethylsiloxane (PDMS) elastomer. *J. Microelectromechan. Systems* **9**, 76–81 (2000).
181. Thorsen, T., Maerkl, S. J. & Quake, S. R. Microfluidic large-scale integration. *Science* **298**, 580 (2002).
182. Unger, M. A., Chou, H. P., Thorsen, T., Scherer, A. & Quake, S. R. Monolithic microfabricated valves and pumps by multilayer soft lithography. *Science* **288**, 113–116 (2000).
183. Woodruff, K. & Maerkl, S. J. A. High-throughput microfluidic platform for mammalian cell transfection and culturing. *Sci. Rep.* **6**, 23937 (2016).
184. Fidalgo, L. M. & Maerkl, S. J. A software-programmable microfluidic device for automated biology. *Lab. Chip* **11**, 1612–1619 (2011).
185. Piraino, F., Volpetti, F., Watson, C. & Maerkl, S. J. A. Digital–analog microfluidic platform for patient-centric multiplexed biomarker diagnostics of ultralow volume samples. *ACS Nano* **10**, 1699–1710 (2016).
186. Miklas, J. W. et al. Bioreactor for modulation of cardiac microtissue phenotype by combined static stretch and electrical stimulation. *Biofabrication* **6**, 024113–024113 (2014).
187. Borysiak, M. D. et al. Simple replica micromolding of biocompatible styrenic elastomers. *Lab. Chip* **13**, 2773–2784 (2013).
188. Borysiak, M. D., Yuferova, E. & Posner, J. D. Simple, low-cost styrene-ethylene/butylene-styrene microdevices for electrokinetic applications. *Anal. Chem.* **85**, 11700–11704 (2013).
189. Guillemette, M. D., Roy, E., Auger, F. A. & Veres, T. Rapid isothermal substrate microfabrication of a biocompatible thermoplastic elastomer for cellular contact guidance. *Acta Biomaterialia* **7**, 2492–2498 (2011).
190. Domansky, K. et al. Clear castable polyurethane elastomer for fabrication of microfluidic devices. *Lab. Chip* **13**, 3956–3964 (2013).
191. Sasaki, H., Onoe, H., Osaki, T., Kawano, R. & Takeuchi, S. Parylene-coating in PDMS microfluidic channels prevents the absorption of fluorescent dyes. *Sensors Actuators B Chem.* **150**, 478–482 (2010).
192. Ren, K., Zhao, Y., Su, J., Ryan, D. & Wu, H. Convenient method for modifying poly (dimethylsiloxane) to be airtight and resistive against absorption of small molecules. *Anal. Chem.* **82**, 5965–5971 (2010).
193. Tran, R. T. et al. Synthesis and characterization of a biodegradable elastomer featuring a dual crosslinking mechanism. *Soft Matter* **6**, 2449–2461 (2010).
194. Davenport Huyer, L. et al. Highly elastic and moldable polyester biomaterial for cardiac tissue engineering applications. *ACS Biomater. Sci. Eng.* **2**, 780–788 (2016).
195. Pan, C., Kumar, C., Bohl, S., Klingmueller, U. & Mann, M. Comparative proteomic phenotyping of cell lines and primary cells to assess preservation of cell type-specific functions. *Mol. Cell. Proteom.: MCP* **8**, 443–450 (2009).
196. Zhao, Y., Korolj, A., Feric, N. & Radisic, M. Human pluripotent stem cell-derived cardiomyocyte based models for cardiotoxicity and drug discovery. *Expert Opin. Drug Safety* **15**, 1455–1458 (2016).
197. Ahadian, S. et al. Organ-on-a-Chip platforms: a convergence of advanced materials, cells, and microscale technologies. *Adv. Healthc Mater.* https://doi.org/10.1002/adhm.201700506 (2017).
198. Unger, R. E., Krump-Konvalinkova, V., Peters, K. & Kirkpatrick, C. J. In vitro expression of the endothelial phenotype: comparative study of primary isolated cells and cell lines, including the novel cell line HPMEC-ST1.6R. *Microvascular Res.* **64**, 384–397 (2002).
199. Baumann, K. Achieving pluripotency. *Nat Rev. Mol. Cell Biol.* **11**, 677 (2010).
200. Saha, K. & Jaenisch, R. Technical challenges in using human induced pluripotent stem cells to model disease. *Cell Stem Cell* **5**, 584–595.
201. Hanna, J. et al. Treatment of sickle cell anemia mouse model with iPS cells generated from autologous skin. *Science* **318**, 1920 (2007).
202. Colman, A. & Dreesen, O. Pluripotent stem cells and disease modeling. *Cell Stem Cell* **5**, 244–247 (2009).
203. Li, Y. Y. & Jones, S. J. M. Drug repositioning for personalized medicine. *Genome Med.* **4**, 27–27 (2012).
204. Evans, W. E. & Relling, M. V. Pharmacogenomics: translating functional genomics into rational therapeutics. *Science* **286**, 487 (1999).
205. van de Stolpe, A. & den Toonder, J. Workshop meeting report Organs-on-Chips: human disease models. *Lab. Chip* **13**, 3449–3470 (2013).
206. Yazawa, M. et al. Using induced pluripotent stem cells to investigate cardiac phenotypes in Timothy syndrome. *Nature* **471**, 230–234 (2011).

207. Moretti, A. et al. Patient-specific induced pluripotent stem-cell models for long-QT syndrome. *N. Engl. J. Med.* **363**, 1397–1409 (2010).
208. Carvajal-Vergara, X. et al. Patient-specific induced pluripotent stem-cell-derived models of LEOPARD syndrome. *Nature* **465**, 808–812 (2010).
209. Wang, G. et al. Modeling the mitochondrial cardiomyopathy of Barth syndrome with induced pluripotent stem cell and heart-on-chip technologies. *Nat. Med.* **20**, 616–623 (2014).
210. Sun, N. et al. Patient-specific induced pluripotent stem cells as a model for familial dilated cardiomyopathy. *Sci. Transl Med.* **4**, 130ra147 (2012).
211. Cong, L. et al. Multiplex genome engineering using CRISPR/Cas systems. *Science* **339**, 819–823 (2013).
212. Hsu, P. D., Lander, E. S. & Zhang, F. Development and applications of CRISPR-Cas9 for genome engineering. *Cell* **157**, 1262–1278 (2014).
213. Völkner, M. et al. Retinal organoids from pluripotent stem cells efficiently recapitulate retinogenesis. *Stem Cell Rep.* **6**, 525–538 (2016).
214. Foster, J. W. et al. Cornea organoids from human induced pluripotent stem cells. *Sci. Rep.* **7**, 41286 (2017).
215. Broutier, L. et al. Human primary liver cancer-derived organoid cultures for disease modeling and drug screening. *Nat. Med.* **23**, 1424 (2017).
216. Broutier, L. et al. Culture and establishment of self-renewing human and mouse adult liver and pancreas 3D organoids and their genetic manipulation. *Nat. Protoc.* **11**, 1724–1743 (2016).
217. Boj, Sylvia, F. et al. Organoid models of human and mouse ductal pancreatic cancer. *Cell* **160**, 324–338.
218. Dedhia, P. H., Bertaux-Skeirik, N., Zavros, Y. & Spence, J. R. Organoid models of human gastrointestinal development and disease. *Gastroenterology* **150**, 1098–1112 (2016).
219. Lancaster, M. A. et al. Cerebral organoids model human brain development and microcephaly. *Nature* **501**, 373 (2013).
220. Chen, Y.-W. et al. A three-dimensional model of human lung development and disease from pluripotent stem cells. *Nat. Cell Biol.* **19**, 542 (2017).
221. Lancaster, M. A. & Knoblich, J. A. Organogenesis in a dish: modeling development and disease using organoid technologies. *Science* **345**, 1247125 (2014).
222. Byun, C. K., Abi-Samra, K., Cho, Y. K. & Takayama, S. Pumps for microfluidic cell culture. *Electrophoresis* **35**, 245–257 (2014).
223. Li, X., Brooks, J. C., Hu, J., Ford, K. I. & Easley, C. J. 3D-templated, fully automated microfluidic input/output multiplexer for endocrine tissue culture and secretion sampling. *Lab. Chip* **17**, 341–349 (2017).
224. Huh, D., Hamilton, G. A. & Ingber, D. E. From 3D cell culture to organs-on-chips. *Trends Cell Biol.* **21**, 745–754 (2011).
225. Wevers, N. R. et al. High-throughput compound evaluation on 3D networks of neurons and glia in a microfluidic platform. *Sci. Rep.* **6**, 38856 (2016).
226. Theberge, A. B. et al. Microfluidic multiculture assay to analyze biomolecular signaling in angiogenesis. *Anal. Chem.* **87**, 3239–3246 (2015).
227. Kim, S., Chung, M., Ahn, J., Lee, S. & Jeon, N. L. Interstitial flow regulates the angiogenic response and phenotype of endothelial cells in a 3D culture model. *Lab. Chip* **16**, 4189–4199 (2016).
228. Osaki, T., Sivathanu, V. & Kamm, R. D. Crosstalk between developing vasculature and optogenetically engineered skeletal muscle improves muscle contraction and angiogenesis. *Biomaterials* **156**, 65–76 (2018).
229. Uzel, S. G. et al. Microfluidic device for the formation of optically excitable, three-dimensional, compartmentalized motor units. *Sci. Adv.* **2**, e1501429 (2016).
230. Patra, B., Peng, C.-C., Liao, W.-H., Lee, C.-H. & Tung, Y.-C. Drug testing and flow cytometry analysis on a large number of uniform sized tumor spheroids using a microfluidic device. *Sci. Rep.* **6**, 21061 (2016).
231. Gruber, P., Marques, M. P., Szita, N. & Mayr, T. Integration and application of optical chemical sensors in microbioreactors. *Lab. Chip* **17**, 2693–2712 (2017).
232. Choi, J.-r., Song, H., Sung, J. H., Kim, D. & Kim, K. Microfluidic assay-based optical measurement techniques for cell analysis: a review of recent progress. *Biosensors Bioelectron.* **77**, 227–236 (2016).
233. Xiao, F., Wang, L. & Duan, H. Nanomaterial based electrochemical sensors for in vitro detection of small molecule metabolites. *Biotechnol. Adv.* **34**, 234–249 (2016).
234. Wang, L., Acosta, M. A., Leach, J. B. & Carrier, R. L. Spatially monitoring oxygen level in 3D microfabricated cell culture systems using optical oxygen sensing beads. *Lab. Chip* **13**, 1586–1592 (2013).
235. Suzuki, H., Hirakawa, T., Watanabe, I. & Kikuchi, Y. Determination of blood pO 2 using a micromachined Clark-type oxygen electrode. *Anal. Chim. Acta* **431**, 249–259 (2001).
236. Bellin, D. L. et al. Integrated circuit-based electrochemical sensor for spatially resolved detection of redox-active metabolites in biofilms. *Nat. Commun.* **5**, 3256 (2014).
237. Wu, M.-H., Lin, J.-L., Wang, J., Cui, Z. & Cui, Z. Development of high throughput optical sensor array for on-line pH monitoring in micro-scale cell culture environment. *Biomed. Microdevices* **11**, 265–273 (2009).
238. Eklund, S. E. et al. Modification of the Cytosensor™ Microphysiometer to simultaneously measure extracellular acidification and oxygen consumption rates. *Anal. Chim. Acta* **496**, 93–101 (2003).
239. Lin, Z., Cherng-Wen, T., Roy, P. & Trau, D. In-situ measurement of cellular microenvironments in a microfluidic device. *Lab. Chip* **9**, 257–262 (2009).
240. Lin, Y., Lu, F., Tu, Y. & Ren, Z. Glucose biosensors based on carbon nanotube nanoelectrode ensembles. *Nano Lett.* **4**, 191–195 (2004).
241. Boero, C. et al. Design, development, and validation of an in-situ biosensor array for metabolite monitoring of cell cultures. *Biosensors Bioelectron.* **61**, 251–259 (2014).
242. Sonker, M., Sahore, V. & Woolley, A. T. Recent advances in microfluidic sample preparation and separation techniques for molecular biomarker analysis: a critical review. *Anal. Chim. Acta* **986**, 1–11 (2017).
243. Xiao, Y., Lubin, A. A., Heeger, A. J. & Plaxco, K. W. Label-free electronic detection of thrombin in blood serum by using an aptamer-based sensor. *Angew. Chem. Int. Ed.* **44**, 5456–5459 (2005).
244. Shin, S. R. et al. Aptamer-based microfluidic electrochemical biosensor for monitoring cell-secreted trace cardiac biomarkers. *Anal. Chem.* **88**, 10019–10027 (2016).
245. Shin, S. R. et al. Label-free and regenerative electrochemical microfluidic biosensors for continual monitoring of cell secretomes. *Adv. Sci.* **4**, 1600522 (2017).
246. Xie, Y. et al. A novel electrochemical microfluidic chip combined with multiple biomarkers for early diagnosis of gastric cancer. *Nanoscale Res. Lett.* **10**, 477 (2015).
247. Henry, O. et al. Organs-on-Chips with integrated electrodes for Trans-Epithelial Electrical Resistance (TEER) measurements of human epithelial barrier function. *Lab. Chip* **17**, 2264–2271 (2017).
248. ávan der Meer, A. D., JungáKim, H., ávan der Helm, M. W. & den Berg, A. Measuring direct current *trans*-epithelial electrical resistance in organ-on-a-chip microsystems. *Lab. Chip* **15**, 745–752 (2015).
249. Murphy, S. V. & Atala, A. 3D bioprinting of tissues and organs. *Nat. Biotechnol.* **32**, 773–785 (2014).
250. Waheed, S. et al. 3D printed microfluidic devices: enablers and barriers. *Lab. Chip* **16**, 1993–2013 (2016).
251. Zhang, Y. S. et al. 3D bioprinting for tissue and organ fabrication. *Ann. Biomed. Engineer.* **45**, 148–163 (2017).
252. Dehne, E.-M., Hasenberg, T. & Marx, U. The ascendance of microphysiological systems to solve the drug testing dilemma. *Future Sci. OA* **3**, FSO0185 (2017).
253. Sager, P. T., Gintant, G., Turner, J. R., Pettit, S. & Stockbridge, N. Rechanneling the cardiac proarrhythmia safety paradigm: a meeting report from the Cardiac Safety Research Consortium. *Am. Heart J.* **167**, 292–300 (2014).
254. US Food and Drug Administration. *Paving the way for personalized medicine*. (FDA, 2013).
255. Conant, G., Ahadian, S., Zhao, Y. & Radisic, M. Kinase inhibitor screening using artificial neural networks and engineered cardiac biowires. *Sci. Rep.* **7**, 11807 (2017).
256. Sun, X. & Nunes, S. S. Biowire platform for maturation of human pluripotent stem cell-derived cardiomyocytes. *Methods* **101**, 21–26 (2016).
257. Marga, F. et al. Toward engineering functional organ modules by additive manufacturing. *Biofabrication* **4**, 022001 (2012).
258. Zhou, M. et al. Development of a functional glomerulus at the organ level on a chip to mimic hypertensive nephropathy. *Sci. Rep.* **6**, 31771 (2016).
259. Wang, L. et al. A disease model of diabetic nephropathy in a glomerulus-on-a-chip microdevice. *Lab. Chip* **17**, 1749–1760 (2017).
260. Lee, J. S. et al. Placenta-on-a-chip: a novel platform to study the biology of the human placenta. *J. Maternal Fetal Neonatal Med.* **29**, 1046–1054 (2016).
261. Booth, R. & Kim, H. Characterization of a microfluidic in vitro model of the blood-brain barrier (μBBB). *Lab. Chip* **12**, 1784–1792 (2012).
262. Brown, J. A. et al. Metabolic consequences of inflammatory disruption of the blood-brain barrier in an organ-on-chip model of the human neurovascular unit. *J. Neuroinflamm.* **13**, 306 (2016).
263. Deosarkar, S. P. et al. A novel dynamic neonatal blood-brain barrier on a chip. *PLoS One* **10**, e0142725 (2015).
264. Prabhakarpandian, B. et al. SyM-BBB: a microfluidic blood brain barrier model. *Lab. Chip* **13**, 1093–1101 (2013).
265. Chung, M. et al. Wet-AMD on a chip: modeling outer blood-retinal barrier in vitro. *Adv. Healthc. Mater.* https://doi.org/10.1002/adhm.201700028 (2017).
266. Kolesky, D. B. et al. 3D bioprinting of vascularized, heterogeneous cell-laden tissue constructs. *Adv. Mater.* **26**, 3124–3130 (2014).
267. Tsvirkun, D., Grichine, A., Duperray, A., Misbah, C. & Bureau, L. Microvasculature on a chip: study of the endothelial surface layer and the flow structure of red blood cells. *Sci. Rep.* **7**, 45036 (2017).
268. Zhang, B., Peticone, C., Murthy, S. K. & Radisic, M. A standalone perfusion platform for drug testing and target validation in micro-vessel networks. *Biomicrofluidics* **7**, 044125 (2013).
269. Ting, L., Feghhi, S., Karchin, A., Tooley, W. & White, N. J. Clot-on-a-chip: a microfluidic device to study platelet aggregation and contractility under shear. *Blood* **122**, 2363–2363 (2013).
270. Lamberti, G. et al. Adhesive interaction of functionalized particles and endothelium in idealized microvascular networks. *Microvascular Res.* **89**, 107–114 (2013).
271. Wang, L. et al. Patterning cells and shear flow conditions: convenient observation of endothelial cell remoulding, enhanced production of angiogenesis factors and drug response. *Lab. Chip* **11**, 4235–4240 (2011).
272. Srigunapalan, S., Lam, C., Wheeler, A. R. & Simmons, C. A. A microfluidic membrane device to mimic critical components of the vascular microenvironment. *Biomicrofluidics* **5**, 13409 (2011).
273. Zhang, Y. S. et al. Bioprinted thrombosis-on-a-chip. *Lab. Chip* **16**, 4097–4105 (2016).
274. Zhang, W. et al. Elastomeric free-form blood vessels for interconnecting organs on chip systems. *Lab. Chip* **16**, 1579–1586 (2016).
275. Yasotharan, S., Pinto, S., Sled, J. G., Bolz, S.-S. & Günther, A. Artery-on-a-chip platform for automated, multimodal assessment of cerebral blood vessel structure and function. *Lab. Chip* **15**, 2660–2669 (2015).
276. Günther, A. et al. A microfluidic platform for probing small artery structure and function. *Lab. Chip* **10**, 2341–2349 (2010).
277. Price, G. M., Chrobak, K. M. & Tien, J. Effect of cyclic AMP on barrier function of human lymphatic microvascular tubes. *Microvascular Res.* **76**, 46–51 (2008).
278. Schaaf, S. et al. Human engineered heart tissue as a versatile tool in basic research and preclinical toxicology. *PLoS One* **6**, e26397 (2011).
279. Yang, X., Pabon, L. & Murry, C. E. Engineering adolescence maturation of human pluripotent stem cell–derived cardiomyocytes. *Circul. Res.* **114**, 511–523 (2014).
280. Bian, W., Jackman, C. P. & Bursac, N. Controlling the structural and functional anisotropy of engineered cardiac tissues. *Biofabrication* **6**, 024109 (2014).
281. Nunes, S. S. et al. Human stem cell-derived cardiac model of chronic drug exposure. *ACS Biomater. Sci. Eng.* **3**, 1911–1921 (2017).
282. Thavandiran, N. et al. Design and formulation of functional pluripotent stem cell-derived cardiac microtissues. *Proc. Natl Acad. Sci. USA* **110**, E4698–E4707 (2013).
283. Guo, X., Gonzalez, M., Stancescu, M., Vandenburgh, H. H. & Hickman, J. J. Neuromuscular junction formation between human stem cell-derived motoneurons and human skeletal muscle in a defined system. *Biomaterials* **32**, 9602–9611 (2011).
284. Davidson, M. D., Lehrer, M. & Khetani, S. R. Hormone and drug-mediated modulation of glucose metabolism in a microscale model of the human liver. *Tissue Eng. Part C Methods* **21**, 716–725 (2015).

285. Chan, T. S., Yu, H., Moore, A., Khetani, S. R. & Tweedie, D. Meeting the challenge of predicting hepatic clearance of compounds slowly metabolized by cytochrome P450 using a novel hepatocyte model, HepatoPac. *Drug Metab. Dispos.* **41**, 2024–2032 (2013).
286. Ballard, T. E. et al. Application of a micropatterned cocultured hepatocyte system to predict preclinical and human-specific drug metabolism. *Drug Metab. Dispos.* **44**, 172–179 (2016).
287. Anastasov, N. et al. A 3D-microtissue-based phenotypic screening of radiation resistant tumor cells with synchronized chemotherapeutic treatment. *BMC Cancer* **15**, 1 (2015).
288. Rimann, M. et al. An in vitro osteosarcoma 3D microtissue model for drug development. *J. Biotechnol.* **189**, 129–135 (2014).
289. Huval, R. M. et al. Microengineered peripheral nerve-on-a-chip for preclinical physiological testing. *Lab. Chip* **15**, 2221–2232 (2015).
290. Liazoghli, D., Roth, A. D., Thostrup, P. & Colman, D. R. Substrate micropatterning as a new in vitro cell culture system to study myelination. *ACS Chem. Neurosci.* **3**, 90–95 (2011).
291. Magdesian, M. H. et al. Atomic force microscopy reveals important differences in axonal resistance to injury. *Biophys. J.* **103**, 405–414 (2012).
292. Belkaid, W. et al. Cellular response to micropatterned growth promoting and inhibitory substrates. *BMC Biotechnol.* **13**, 86 (2013).
293. Magdesian, M. H. et al. Rapid mechanically controlled rewiring of neuronal circuits. *J. Neurosci.* **36**, 979–987 (2016).
294. Khoshakhlagh, P. & Moore, M. J. Photoreactive interpenetrating network of hyaluronic acid and Puramatrix as a selectively tunable scaffold for neurite growth. *Acta Biomaterialia* **16**, 23–34 (2015).
295. Peyrin, J.-M. et al. Axon diodes for the reconstruction of oriented neuronal networks in microfluidic chambers. *Lab. Chip* **11**, 3663–3673 (2011).
296. Deleglise, B. et al. β-Amyloid induces a dying-back process and remote *trans*-synaptic alterations in a microfluidic-based reconstructed neuronal network. *Acta Neuropathol. Commun.* **2**, 145 (2014).
297. Taylor, A. M. et al. A microfluidic culture platform for CNS axonal injury, regeneration and transport. *Nat. Methods* **2**, 599–605 (2005).

Acknowledgements
The authors thank M. Lecce and L. D. Huyer for helping with the editing of this manuscript. This work was made possible by the National Sciences and Engineering Research Council of Canada (NSERC) Postgraduate Scholarships-Doctoral Program awarded to B.F.L.L., Alexander Graham Bell Canada Graduate Scholarships-Doctoral Program awarded to A.K. and the Canadian Institutes of Health Research (CIHR) Banting Postdoctoral Fellowship to B.Z. This work was also funded by the CIHR Operating Grants (MOP-126027 and MOP-137107), NSERC Discovery Grant (RGPIN-2015-05952), NSERC Steacie Fellowship (SMFSU 4620), Heart and Stroke Foundation Grant-in-Aid (G-16-00012), NSERC-CIHR Collaborative Health Research Grant (CHRPJ 4937) and NSERC Strategic Grant (STPGP 5066) to M.R.

Author contributions
B.Z., A.K. and B.F.L.L. wrote and edited the manuscript. M.R. supervised the work and edited the manuscript.

Competing interests
B.Z. and M.R. hold equity in TARA Biosystems Inc.

Publisher's note
Springer Nature remains neutral with regard to jurisdictional claims in published maps and institutional affiliations.

RELATED LINKS
American Institute for Medical and Biological Engineering (AIMBE): http://aimbe.org
Comprehensive In Vitro Proarrhythmia Assay (CiPA): http://cipaproject.org
IQ Consortium: https://iqconsortium.org